New age constraints for glacial terminations IV, III, and III.a based on Western Mediterranean speleothem records

Judit Torner[1], Isabel Cacho[1], Heather Stoll[2], Ana Moreno[3], Joan O. Grimalt[4], Francisco J. Sierro[5], Joan J. Fornós[6], Hai Cheng[7], and R. Lawrence Edwards[8]

[1]GRC Geociències Marines, Dept. de Dinàmica de la Terra i de l'Oceà, Universitat de Barcelona, Barcelona, 08028, Spain
[2]Department of Earth Sciences, ETH Zúrich, 8092, Switzerland
[3]Departamento de Procesos Geoambientales y Cambio Global, 639/, CSIC, 50059 Zaragoza, Spain
[4]Institute of Environmental Assessment and Water Research (IDAEA-CSIC), Barcelona, 08034, Spain
[5]Departmento de Geología, Universidad de Salamanca, Salamanca, 37008, Spain
[6]Earth Sciences Research Group. Departament de Biologia, Universitat de les Illes Balears, 07122 Palma (Mallorca), Spain
[7]Institute of Global Environmental Change, University of Xi'an Jiaotong, 710049 Xi'an, China
[8]Department of Earth Sciences, University of Minnesota, MN 5545, USA

Correspondence to: Judit Torner (j.torner@ub.edu)

Abstract. The full understanding of climate feedbacks responsible for the amplification of deglaciations requires robust chronologies for these climate transitions, but, in the case of marine records, radiocarbon chronologies are possible only for the last glacial termination. Although the assumed relationships between the marine isotopic record and the orbital parameters provide a first order chronology for glacial terminations, an independent chronological control allows the relationships between orbital forcing and the climate response to be evaluated over multiple previous terminations. To assess this, we present geochemical records from the western Mediterranean, including two speleothems and one marine sediment core. The most notable speleothem, so-called RAT, established a new long terrestrial climate record for this region, spanning Marine Isotope Stages 11 to 7. Its absolute U/Th dates provide an exceptional chronology for the glacial terminations IV, III, and III.a. The onset of these three glacial terminations was marked by rapid $\delta^{18}O$ depletions, reflecting ocean freshening by ice melting, thus providing an excellent tie point for regional marine records also sensitive to such freshening. This is exemplified by new $\delta^{18}O$ data of the ODP 977 site from the Alboran Sea, where the speleothem chronology was employed to adjust its age model. The new chronologies reveal an earlier onset of the deglacial melting for the TIV and TIII.a in contrast to the generally accepted marine chronologies and indicate that the duration of these deglaciations was variable, with TIV particularly longer (~20 kyr). This study also supports that the onset of deglacial melting always occurred during declining precession index while a nonunique relation occurred with the obliquity parameter.

1 Introduction

Glacial-interglacial transitions exemplify the highest amplitude of climate changes along the Late Quaternary and involve intense and fast processes of ice-sheet melting that led to rapid sea level rise (PAGES, 2016). Although increasing northern hemisphere summer insolation (NHSI) is considered the main driver for deglaciations, internal feedbacks from the Earth's climate system were crucial to trigger glacial terminations. (Cheng *et al*., 2009; Drysdale *et al*., 2009; Tzedakis *et al*., 2012; Barker *et al.,* 2021). The consequences of the insolation rise depended on the actual extent of the ice-sheet build-up during the preceding glacial period, determining the main features of terminations (Tzedakis *et al.,* 2017). Ice-sheet instability and intense events of massive icebergs released into the N Atlantic, named Henrich-like events, are considered characteristic features of deglaciation (Barker *et al*., 2015, 2019, 2021; Hodell *et al*., 2013, 2023) and have been well-documented through ice rafting debris (IRD) records in the N Atlantic (Hodell *et al*., 2008; Barker *et al*., 2011). The consequent North Atlantic freshening caused by ice melting became the trigger for powerful feedback processes inducing glacial terminations. The freshwater discharge allowed surface water stratification and provoked the displacement of the deep-water formation, disturbing the strength of the Atlantic Meridional Overturning Circulation (AMOC) (Rahmstorf 2002). This, in turn, changed the interhemispheric heat transport, inducing a rapid cooling in the North Atlantic region, whereas Antarctica gradually warmed. The asymmetry in the hemispheric heat transport (the bipolar-seesaw) and its influence on the atmospheric CO_2 rise was also a fundamental requirement to enter into a deglaciation (Cheng *et al*., 2009; Barker *et al*., 2011, 2019, 2021; Tzedakis *et al*., 2012). Thus, variations in the AMOC and greenhouse gases explain much of the variability in global climate during deglaciations (Clark *et al*., 2012). In parallel to the weakening of the AMOC, albedo changes due to the reduction of continental ice sheet extent operated as secondary internal feedback or amplifier. At the end of deglaciations arises the characteristic abrupt warming leading to the onset of interglacial periods but, the sea level highstand marking the interglacial conditions, occurred systematically a few thousand years after the maximum in NH summer insolation due to the slow response of the ice sheets to insolation (PAGES, 2016). Several warm marine isotopic substages are considered interglacial acmes or peaks of optimum climate conditions (the MIS 7a-c, 7e, 9e, and 11c within them). However, temporal and geographical asynchronies in the precise definition of their boundaries between marine and terrestrial records or even different proxies within the same archives pose a challenge to resolving the feedbacks acting in these transitional periods (Shackleton, 1969, 2003; Sanchez-Goñi *et al*., 1999). These feedbacks responsible for past deglacial warming can also play a role in the ongoing situation of climate change. The increase in atmospheric CO_2 due to anthropogenic emissions, the reduction in earth albedo resulting from ice melting, and even the weakening of the AMOC are currently in operation (IPCC, 2023; Boers, 2021). Studying past glacial terminations provides unique examples for elucidating the role that these internal components on Earth's climate system had during past periods of global climate warming, a test ground for better contextualizing current climate change.

Astronomically-tuned marine sediment records provided fundamental information to understand the evolution of the continental ice sheets in the past. Globally averaged $\delta^{18}O$ stacks from benthic foraminifera, reflecting changes in ice-sheet build-up and deep ocean temperature, have provided a global chronological framework for correlating marine sediment sequences, and the marker is its global signal driven by changes in the ice-sheet build-up. (Imbrie *et al*, 1984; Martinson *et al*., 1987; Lisiecki and Raymo, 2005). However, the chronology applied to such stacks is based on the assumption of a stationary relationship between insolation and ice volume changes and does not account for suborbital climate influence in the time sequences of each glacial termination (Hodell *et al*., 2015). While also reflecting ice volume cycles, the seawater oxygen isotopic signal ($\delta^{18}O_{sw}$) from planktonic records can be overprinted by regional temperature or hydrographic changes challenging its use as an isotopic chronostratigraphic tool (Rohling *et al*., 2015). Hence orbitally dependent marine isotopic chronologies are limited in resolving precise age constriction of key climate periods, such as glacial-interglacial transitions, complicating any interpretation in terms of orbital forcing.

A growing number of studies use absolute dating from speleothems to anchor the marine records and achieve astronomically independent age models (e.g., Grant *et al*., 2012; Cheng *et al*., 2016). Speleothems with a relatively unambiguous climatic interpretation of their proxies spanning continuously several glacial-interglacial cycles are restricted to a few studies. For instance, speleothem records from America support orbital parameters as the predominant driver of glacial terminations, although they are limited to the two most recent cycles (Cruz *et al*., 2005, 2009; Moesley *et al*., 2016). Another notable example is the case of Chinese speleothems that provided a great paleoclimatic assembled record of the Asian monsoon lasting 640 kyr and encompassing various deglaciations (Yuan *et al*., 2004; Cheng *et al*., 2006, 2009, 2016). They even reported first insights into the existence of the extra glacial termination TIII.a, which reproduces patterns of events equivalent to other glacial terminations despite being amid MIS 7 (Cheng *et al*., 2009). Superimposed on a strong precessional $\delta^{18}O$ signal forced by regional insolation and sea surface temperature gradients, these precisely dated speleothem records from Sanbao cave in China show positive $\delta^{18}O$ anomalies interpreted to reflect changes in the position and timing of monsoon rainfall coincident with the weakening of the AMOC in the North Atlantic (Wang, 2001; Cheng *et al*., 2009; Cai *et al.,* 2015; Barker *et al*., 2021; Jian *et al*., 2022). If AMOC weakening is linked to glacial meltwater release in the North Atlantic, these records may, therefore, provide indirect indicators of the chronology of glacial terminations. However, the distinctive freshening signature of the glacial terminations and therefore the specific time sequence of its events cannot be recorded in these speleothems located far from the N Atlantic water sources. Hence, well-constrained speleothem records capable of recording the North Atlantic deglacial features through its isotopic signature would be advantageous to establish independent chronology on North Atlantic marine sequences and clarify the forcings of deglaciations. In this respect, the first high-resolution speleothem records successfully used to tune marine records were collected in the NW Iberia peninsula and documented rapid North Atlantic ice sheet melting spanning the two ultimate glacial terminations (TI and II) at millennial-centennial timescale (Stoll *et al.,* 2022).

Regarding the Mediterranean region, available speleothem records that can be potentially used for marine alignments are mostly restricted for the two most recent deglaciations (e.g. Bar-Matthews *et al.*, 1999, 2000 and 2003; Drysdale *et al.*, 2009; Tzedakis *et al.*, 2018). In the western Mediterranean basin, only the Ejulve speleothem record from the eastern Iberian Peninsula detected millennial-scale events related to AMOC slowdowns at TIII (Pérez-Mejías *et al.*, 2017). While speleothems spanning TIV and TV remain elusive in the Mediterranean context (Kaushal *et al.*, 2024). This study presents two new speleothem records from the Balearic Islands located in the western Mediterranean region (Fig. 1). The VALL 2 speleothem was recovered from Mallorca Island and encompassed the TV. Whereas the RAT speleothem, recovered from Minorca Island, encompassed two glacial-interglacial cycles with the chronologies for the glacial terminations TIV, TIII, and TIII.a well-constrained. Hence the RAT speleothem offers a unique continuous record not provided by any existing stalagmite archive within this region. A geochemical multiproxy approach has been applied in these two speleothems to investigate climate variability with a special focus on their glacial terminations. The studied deglaciations present different intensities and durations and open an opportunity to investigate the relationship between orbital parameters and paleoclimatic records. We apply the RAT chronology to newly acquired planktic isotope measurements from the ODP 977 site in the Alboran Sea, highlighting the potential of this speleothem record as a referential base for marine chronologies. This approach aims to avoid the circularity of trying to understand the drivers and thresholds of climate variability using marine chronologies depending on orbital tuning.
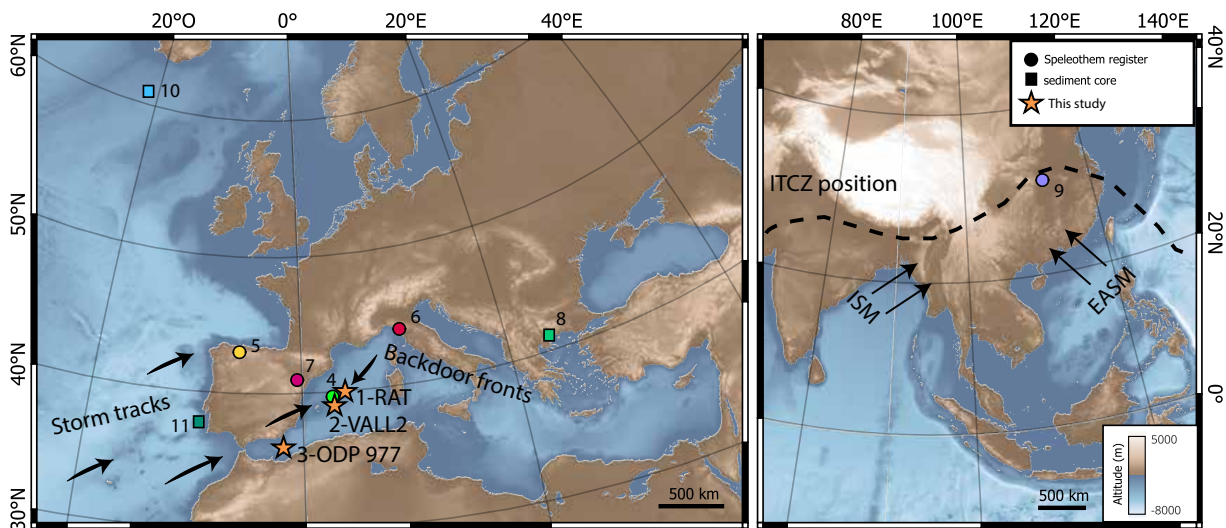
Figure 1: Map showing the location of this study records: 1) Murada cave, in Menorca Island, where the RAT speleothem was recovered. 2) Vallgornera cave in Mallorca Island, where the VALL 2 speleothem was recovered. 3) The marine sediment ODP 977 site. Other sites discussed in the text are also situated: 4) Campanet cave on Mallorca Island (Dumitru *et al.*, 2018). 5) NISA and Garth speleothem records from north Iberia caves (Stoll *et al.*, 2015 and 2022). 6) Corchia cave (Drysdale *et al.*, 2004 and Tzedakis *et al.*, 2018). 7) Ejulve cave (Pérez-Mejías *et al.*, 2017). 8) The Tenaghi Philippon arboreal pollen record (Tzedakis *et al.*, 2006). 9) Sanbao speleothem record (Cheng et al., 2009, 2016). 10) The ODP 983 site (Barker *et al.*, 2015, 2019, 2021). 11) The MD01-2444 marine core (Tzedakis *et al.*, 2018; Hodell *et al.*, 2023). The map shows the dominant atmospheric circulation that brings moisture

120   **to the Balearic Islands (via Mediterranean backdoor cold fronts and winter storm tracks). While moisture in Asia is related to the dynamics of the East Asian Summer Monsoon (EASM) and the Indian Summer Monsoon (ISM), which depends on the Intertropical Convergence Zone (ITCZ). The map shows the modern average position of the ITCZ in summer.**

2 Material and Methods

2.1 Cave settings and regional hydroclimate

125   The speleothem called Ratpenat (RAT) was collected from inside *Murada* cave, in Menorca (Fig. 1). The *Murada* cave is located close to the coast and at little altitude, 80 m a.s.l., in the southwest area of the island (39°57'58''N; 3°57'53''E). This cave is the largest in the *Barranc d'Algendar*, which is a canyon formed by a ravine cutting Miocene calcarenite rocks where a karst was developed. Nowadays, this cave represents a fossil level of the karst drainage conduit. The RAT speleothem was found broken in two pieces, which were matched in the cave. The VALL 2 speleothem grew inside the Es Pas de Vallgornera

130   cave, which is located in the southern part of Mallorca Island (39° 22' 00'' N, 2° 52' 25'' E) (Fig. 1). This cave was also developed in upper Miocene rocks and consists of more than 67 km conduits and chambers, some of them flooded. Sea level reconstruction by means of overgrowths on speleothems has been previously studied in this cave (Dorale *et al*., 2010).

According to the Köppen climate classification, the Balearic Islands present temperate climate (Csa) with seasonal rainfall,

135   intense storms in autumn, and dry/hot summers that cause the lack of permanent watercourses. The two main origins of the precipitation on the western Mediterranean Sea are the Mediterranean Sea itself and the tropical–subtropical North Atlantic corridor via the dominant eastward atmospheric circulation, leading storm tracks reaching the Mediterranean (Gimeno *et al*., 2010; Nieto *et al*., 2010; Krklec and Domínguez-Villar, 2014; Dumitru *et al.*, 2017; Moreno *et al.,* 2021). However, the major source of moisture for precipitation in the Mediterranean surrounding land area has been identified as the basin itself (Schicker

140   *et al*., 2010). Particularly in the Balearic Islands location, the moisture is provided by evaporation over the Mediterranean because of the occurrence of backdoor cold fronts related to easterly advection leading to heavy precipitation in autumn (Millan *et al*., 2005; Moreno *et al.,* 2021). The Mediterranean region has important climate contrasts among different nearby areas because it is a transitional zone between subtropical and midlatitude temperate regimens (Lionello, 2012). While the northern part of the Mediterranean region is strongly linked to midlatitude variability, mostly characterized by the North Atlantic

145   Oscillation, the southern and eastern parts are exposed indirectly to the influences of the Inter-Tropical Convergence Zone dynamics (ITCZ).

2.2 Geochemical Analyses of Speleothems

2.2.1 Geochronology

In order to determine the absolute ages, both speleothems were longitudinally cut with a saw, taking into account the

150   morphology and the growth axis. The sampling for measuring uranium and thorium isotopes was designed considering the

layering to detect possible hiatuses and changes in growth rates. RAT is a 50 cm long speleothem broken at the top; a 2cm calcite piece was missing when the sample was found in the cave. It does not reveal important changes in the orientation of the growth axis, but presents a prominent orange-brown layer at 14 cm from the tip and white layers at 19 and 33 cm (Fig. 2).
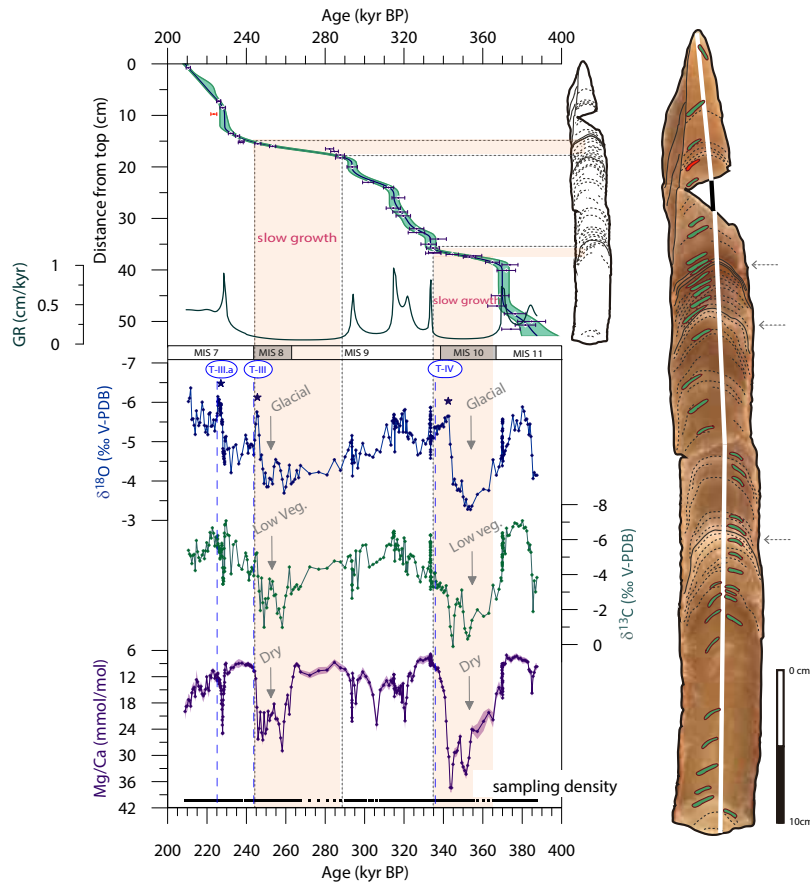
Figure 2: At the right is an image of the RAT speleothem showing the positions of the radiometric dates sampled for creating the age model (green) and the reversal not used (red). The growth axis path used for the geochemical analyses is highlighted with a white line. At the top left, the age model acquired by StalAge (dark blue line) and the original U/Th dates for the RAT speleothem (dark blue dots) are plotted with the associated errors (error bars and green area). RAT growth rates are shown in dark green. In the lower panel, the results of $\delta^{18}O$, $\delta^{13}C$, and Mg/Ca ratios accompanied by uncertainties represented as a shaded area. Note that the three parameters are plotted with a reversed axis. The stars highlight negative $\delta^{18}O$ anomalies mentioned in the main text. The pink bars highlight slow growth rate periods, and the dashed grey line points to major color changes of the speleothem layers, also noted as dashed grey arrows in the image.

The VALL2 speleothem is a wide dark-brown speleothem of 22 cm long (appendix Fig. B1). The color at the bottom of the speleothem is light brown with a porous texture that, towards the top, becomes darker and less porous. The axis presents several changes in the growth direction and possible discontinuities are characterized by light layers. After the last main discontinuity,

the speleothem presents two independent growths. The axis selected to accomplish the analyses follows the most developed axis of the last two growths.

170 Samples for U/Th analyses were milled with a 2 mm diameter tungsten carbide micro-drill under a laminar airflow cabinet to prevent contamination. About 100-200 mg of carbonate powder was obtained for each sample. The chemical procedure for isolating uranium and thorium elements was performed in the ultra-clean laboratory at the University of Minnesota and Xi'an Jiaotong University, applying the methodology previously described by Shen *et al*., (2002) and Cheng *et al*., (2009) (Appendix A). Several blanks were performed routinely for each laboratory sampling set. The radiogenic isotopes of U and Th were

175 analyzed using a parallel ion-counting Multi Collector Inductively Coupled Plasma Mass Spectrometry (MC-ICP-MS) with a *Finnigan Neptune* model at both universities. The results of these analyses and the absolute dates are detailed in Table A1. The speleothem depth-age models were performed with the R software and the StalAge package (Scholz, 2011), using 39 radiometric dates for RAT and 12 for VALL 2. The RAT speleothem provided a consistent chronology with a few single dates exceeding the final modeled dating uncertainty. It presents a remarkably precise age model with absolute uncertainties being

180 even smaller in the youngest part of the speleothem (Fig. 2). The dates obtained from the VALL 2 speleothem are approaching the limits of the U-series dating technique, thereby resulting in significant uncertainties, being even larger in the oldest section of the speleothem, where the growth rate is higher (appendix Fig. B1). The growth rates range between 0.02-1.2 cm/kyr for VALL 2 and 0.07-1.7 cm/kyr for RAT.

2.2.2 Geochemical measurements

185 Stable isotopes and trace elements have been measured on aliquots of the same powder sample in both speleothems. The $\delta^{18}O$, $\delta^{13}C$, and Mg/Ca ratios have been compared in detail to evaluate their paleoclimatic signals. Samples were drilled using a 0.5 mm diameter tungsten carbide dental burr along the speleothem growth axis. Sample resolution is 2 mm in VALL 2 and 2.5 mm in RAT. However, samples are spaced every 0.5 mm during glacial terminations in RAT speleothem to increase temporal resolution due to low growth rates, ensuring that events are captured by more than one measurement.

190

The $\delta^{18}O$ and $\delta^{13}C$ measurements were performed with 50 µg of carbonate powder and were accomplished on a Finnigan-MAT 252 mass spectrometer (IRMS) at the Scientific and Technological Centres of the University of Barcelona (CCiT-UB). This mass spectrometer is coupled in a single acid bath CarboKiel‑III carbonate preparation device to convert solid carbonate samples into simple gas (CO_2) before entering into the ion source of the IRMS. Analytical uncertainties were obtained utilizing

195 two in-house carbonate standards that were calibrated to NBS-19 international standard (Coplen, 1996). The uncertainties were ≤ 0.04 ‰ VPDB for $\delta^{13}C$ and 0.08 ‰ VPDB for $\delta^{18}O$.

Around 3 mg of carbonate powder was used to measure Ca, Mg, and other trace elements such as Ba and Sr to obtain element/calcium ratios. The powder was directly dissolved with 2 ml of ultra-pure 2% HNO_3 (with Rh and Sc as internal standards) and centrifuged to prevent possible lithic particles or impurities in the solution before the analyses. These samples were analyzed employing inductively coupled plasma mass spectrometry (ICP-MS), an Agilent 7500CE model, at the CCiT-UB. Possible contamination was controlled by means of chemistry blank analyses on random days. An in-house high-purity standard solution was measured routinely every four samples to control the accuracy of the measurements. According to the in-house standard analysis, the external reproducibility obtained for the speleothem analyses was 0.86% (%, 2-sigma).

2.3 δ^{18}O Analyses in Planktic Foraminifera from ODP 977 Site

ODP Site 977 was retrieved during LEG 161 of the Ocean Drilling Program on board the *JOIDES Resolution* cruise. It was located halfway between the Spanish and Algerian coasts, in the eastern sub-basin of the Alboran Sea, at 36°01.92'N and 1°57.32'W, and from a water depth of 1984 m b.s.l. (Fig. 1). This study extends the oxygen isotope data obtained in previous studies of this sediment core (Martrat *et al.,* 2004 and 2007; González-Mora *et al.,* 2008; Torner *et al.*, 2019; Azibeiro *et al.*, 2021). The ODP 977 age models of all these different studies are mostly based on the original age model from Martrat *et al.*, 2004 which is established on the correlation between its *Globigerina bulloides* δ^{18}O curve and the SPECMAP stacked curve (Martinson *et al.*, 1987). However, in Torner *et al.*, (2019) some additional tie points were used to align the TII with other Mediterranean cores radiometrically tuned with speleothems. Whereas Azibeiro *et al.*, (2021) adjusted the age model along the TV by aligning its alkenone-based SST record to North Atlantic mid-latitude temperature records.

Stable isotopes on planktic foraminifers were performed on handpicked specimens of *G. bulloides*. Shells were crushed between two glass plates to open the chambers and favor the following clay removal. Afterward, samples were cleaned with methanol and sonicated for a few seconds. The supernatant solution was removed with a micropipette and the samples were finally dried. The measurements were accomplished by isotope ratio mass spectrometry at the CCiT-UB using the same analytical method that was previously explained for speleothems analyses.

3 Results and Discussion

3.1 The climate signal in the speleothems

Mg/Ca ratios and stable isotopes in both speleothems reveal climate variability in the western Mediterranean region. According to the obtained depth-age models, the VALL 2 spans from 530 to 345 ka BP (MIS 13-11), encompassing the glacial termination V. While RAT spans from 387 to 209 ka BP (MIS 11-7), covering continuously an exceptional long-time-interval (178 kyr) that includes three glacial Terminations (TIV, TIII, and TIII.a). Glacial conditions are characterized by slower growth rates and high δ^{18}O, δ^{13}C, and Mg/Ca, while the warm marine isotopic stages feature low isotopes and Mg/Ca ratios (Fig. 2 and appendix B1). The RAT record presents an overall variation of 3.2‰, 6.3‰ and 24.6 mmol/mol for δ^{18}O, δ^{13}C, and Mg/Ca,

respectively. And the overall variation is 3.4 ‰, 3.8 ‰, and 15.7 mmol/mol in the VALL 2 speleothem. Given the insufficient robustness of the VALL 2 age model for the precise evaluation of climatic events, the discussion is primarily focused on the RAT results.

The Mg/Ca ratio in speleothems is sensitive to variations in the precipitation/evaporation balance, reflecting changes in the amount of water infiltrating into the karst system. Frequently, arid conditions, characterized by reduced water infiltration, may increase the groundwater residence time in the karst and even reduce drip rates in the caves (Fairchild *et al.,* 2000). This scenario provides an opportunity to enhance the degassing of groundwaters, thereby facilitating carbonate precipitation prior to the arrival of drip water at the surface of the speleothem. This process, known as prior calcite precipitation (PCP), can also be favored by reductions in the partial pressure of CO_2 (pCO_2) within the cave atmosphere. Ventilation typically reduces the CO_2 levels in the cave and occurs when external cooling provokes an exchange of air between the internal and external atmosphere. This mechanism typically occurs on a seasonal scale, and, presuming that the cave structure has remained constant over time, this influence would persist throughout glacial and interglacial periods, exerting a minor impact on the millennial timescale. Moreover, cold and arid conditions cause a decline in vegetation activity, leading to lower respiration rates and diminished CO_2 liberation. Briefly, processes that reduce pCO_2 in the karstic system support PCP. This PCP can preferentially remove Ca from the drip waters, consequently elevating the trace element/Ca ratio of all incompatible elements in the dripwaters, such as Mg/Ca, Sr/Ca, and Ba/Ca. When the partitioning coefficients of Mg, Sr, and Ba in stalagmite calcite are relatively stable, the speleothem Mg/Ca, Sr/Ca, and Ba/Ca reflect this dripwater PCP signature. The RAT Sr/Ca and Ba/Ca records show similar temporal variations as Mg/Ca variability (appendix Fig. C1), suggesting that all three elements are dominated by a common process of PCP. The magnitude of change in Mg/Ca is much larger than would arise due to temperature-driven changes in Mg partitioning, which in any case would elevate Mg incorporation during warm interglacials, in contrast to the observed pattern. PCP can also be enhanced by higher dripwater saturation states even with constant drip rates (Stoll *et al*., 2012), but the observation of maximum PCP during cold glacial periods characterized by lower soil CO_2 due to diminished microbial activity and vegetation respiration rates and likely lower initial dripwater saturation suggests that elevated glacial PCP is caused by slower drip rates and driven by lower infiltration and lower precipitation-evapotranspiration.

Speleothem $\delta^{13}C$ can also reflect hydroclimate variations. The initial $\delta^{13}C$ of the drip water reflects a mixing signal derived from the carbon isotopic composition signatures of limestone, atmospheric CO_2, and the biogenic soil gas proceeding from both the microbial activity and the vegetation respiration (Hellstrom *et al.*, 1998). Soil autotropic and heterotrophic respiration typically have lower $\delta^{13}C$ values. Hence, cold and dry conditions can depress soil respiration rates and contribute to an increase in the $\delta^{13}C$. Likewise, the concentration of atmospheric CO_2 (with higher $\delta^{13}C$) would be proportionally higher than the relatively low biogenic carbon signature in the soil gas, elevating even more the $\delta^{13}C$ values. Is for that reason that many mid-latitude speleothem studies interpret high $\delta^{13}C$ as reflecting reduced soil/vegetation activity (Genty *et al.,* 2013; Moreno *et al.,* 2010; Bartolomé *et al.,* 2015; Pérez-Mejias *et al*., 2017). Additionally, slowed drip rates during dry periods may contribute to

greater PCP, which also causes dripwater to evolve to higher $\delta^{13}C$ due to the gradual loss of the light isotope. Thus, via these two processes (initial dripwater changes and PCP) dry conditions may contribute to higher speleothem $\delta^{13}C$. In the RAT record, while cold temperatures likely depressed soil respiration during glacials and contributed to the high $\delta^{13}C$, the general co-variation between Mg/Ca and $\delta^{13}C$ suggests that the high glacial $\delta^{13}C$ also reflects dryer conditions contributing to low soil CO_2 and slower drip rates favouring more extensive PCP. In another speleothem record from Mallorca, high $\delta^{13}C$ was similarly interpreted to reflect low biogenic CO_2 productivity in soil and/or a short water residence time, reflecting dry conditions (Dumitru *et al.,* 2018). The RAT-$\delta^{13}C$ signal shows a smoothed signal with respect to the Mg/Ca during glacial terminations, suggesting a slower response of the vegetation compared with precipitation rises (Fig. 2). The MIS 11, 9, and 7 were characterized by enhanced precipitation conditions that led to higher soil respiration activity under more extensive vegetation.

The $\delta^{18}O$ RAT record is marked by higher $\delta^{18}O$ during glacials and lower $\delta^{18}O$ during interglacials (Fig. 2). On a global scale, the retreat of large continental Northern Hemisphere ice volume and release of meltwater lowers the $\delta^{18}O_{sw}$ in the surface ocean. This lower $\delta^{18}O_{sw}$ causes a corresponding decrease in the $\delta^{18}O$ of rainfall and the drip waters from which the speleothem is formed, lowering the speleothem $\delta^{18}O$. Over the most recent glacial cycles, the North Atlantic experiences a greater amplitude change in $\delta^{18}O_{sw}$ than the globally averaged surface ocean (Waelbroeck *et al*., 2014). Whereas in some regions, major changes in atmospheric circulation patterns cause additional larger changes in rainfall $\delta^{18}O$ which significantly exceed the effect of the surface $\delta^{18}O_{sw.}$ In coastal regions of the North Atlantic, the change in surface ocean isotopic composition is a dominant component of speleothem $\delta^{18}O$ variations over glacial terminations. Comparison of independently dated marine $\delta^{18}O_{sw}$ with speleothem $\delta^{18}O$ records from NW Iberia showed that the speleothem $\delta^{18}O$ matched the timing and amplitude of the $\delta^{18}O_{sw}$ shift in the eastern North Atlantic during Termination I (Stoll *et al.,* 2022). Furthermore, several studies demonstrate that the N Atlantic $\delta^{18}O_{sw}$ signal, changed by those freshwater inputs, was transferred into the Mediterranean Sea (Cacho *et al*., 1999; Sierro *et al*., 2005; Jiménez-Amat and Zahn, 2015; Marino *et al*., 2015). Over Termination I, the North Atlantic $\delta^{18}O_{sw}$ decreased rapidly around 16 ka and between 12 and 10 ka, and these two shifts are also recorded in the Alboran Sea as well as around Menorca (appendix Fig. D1). Consequently, we propose that the RAT $\delta^{18}O$ records the change in $\delta^{18}O_{sw}$ in the moisture source area for the precipitation, encompassing both, global changes of the $\delta^{18}O_{sw}$ at a large scale, and superimposed, the freshening signal transmitted to the Mediterranean Sea during deglaciations. This is also supported by the evaluation of the isotopic composition of rainfall waters and cave dripwaters in Mallorca, which points to the western Mediterranean as the dominant source for moisture uptake in coastal caves (Dumitru *et al*., 2017). The cave location of this study, close to the coast and at a low altitude above sea level, should minimize distillation processes, and therefore RAT $\delta^{18}O$ captures the signal of the moisture source, surface water mostly from the Western Mediterranean.

3.2 Mediterranean precipitation modulated by precession

The RAT Mg/Ca record shows a clear precession pattern. Low Mg/Ca, indicating enhanced precipitation, coincides with precession minima, which are times of high north hemisphere summer insolation (NHSI) (Fig. 3, pink bars) and vice versa for

drier periods. The most humid periods are recorded during the strong precession minima of marine isotopic sub-stages MIS 9e and 9a, and MIS 7e. MIS 11a shows similar humidity despite a moderate precessional minimum. The low resolution of the Mg/Ca record during the MIS 9a precludes us from evaluating its duration and structure. In the better resolved interglacial acmes MIS 9e and MIS 7e, we estimate a duration of ~10 kyr. These orbitally paced changes in Mediterranean precipitation are explained because minima precession led to higher seasonality (high NHSI - low NHWI), which intensified wintertime storm tracks and increased the Mediterranean precipitation. Additionally, higher air-sea temperature gradients enhanced evaporation from the Mediterranean basin itself, leading to greater local convective precipitation (Kutzbach et al., 2014; Wagner *et al.*, 2019; García-Alix *et al.,* 2021).
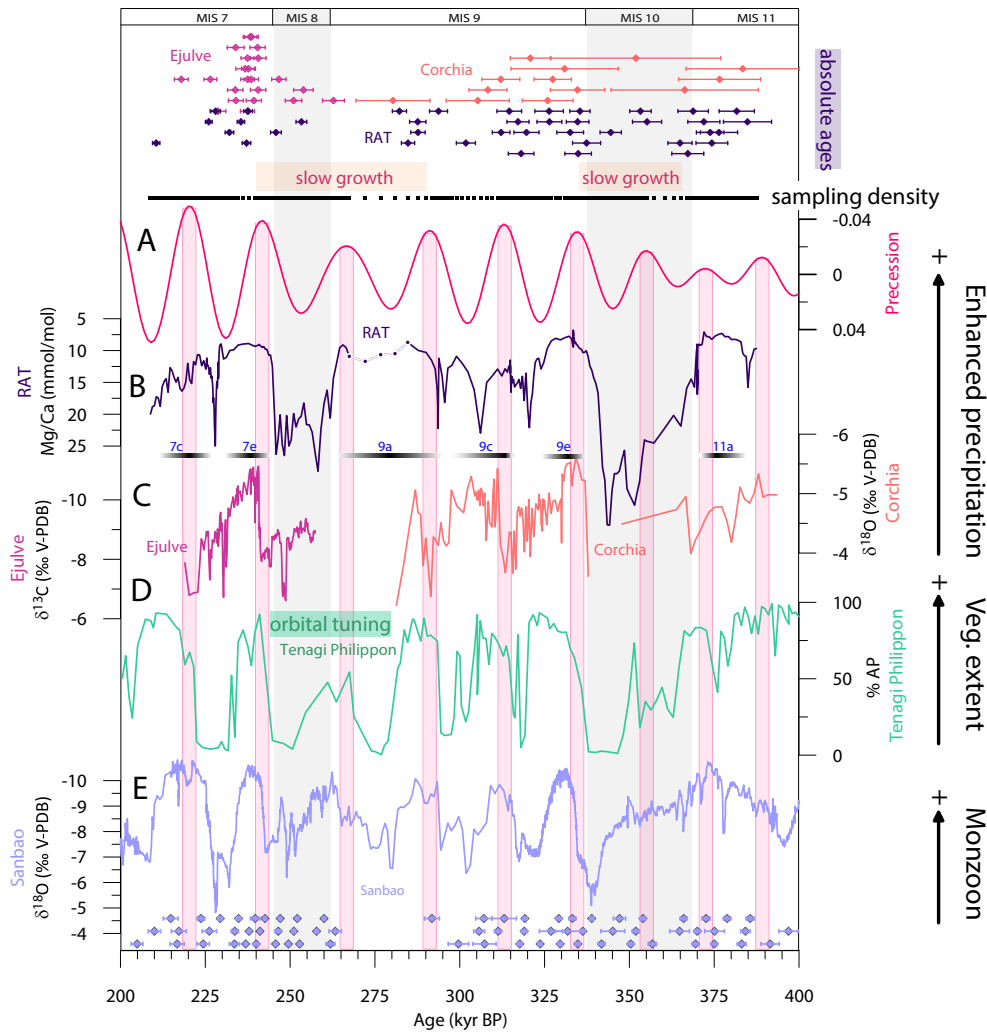
This new uninterrupted record covers enough time length to confirm the precession imprint for the first time in a Mediterranean speleothem. Other European speleothems have also recorded enhanced precipitation during precession minima of the studied interglacials, however, they provide shorter records. The iconic δ^{18}O record of the Antro del Corchia cave, from Italy, shows periods of greater humidity in line with those recorded in RAT during the MIS 9 (Drysdale *et al.*, 2004; Tzedakis *et al.*, 2018). However, higher U/Th date uncertainties could account for some chronological discrepancies (Fig. 3). The increment in moisture availability in western Italy was attributed to regional warm SST that led to enhanced evaporation (Drysdale *et al.,* 2004). Carbon isotope records from other European speleothems are more complex to interpret without accompanying trace elements, but the trends are consistent with warmth and/or greater humidity during MIS 7e. The δ^{13}C speleothem record from the Ejulve cave, in the north-eastern Iberian Peninsula, shows lower values during the MIS 7e (Fig. 3) and is interpreted as a proxy of vegetation productivity (Pérez-Mejias *et al.,* 2017). Considering that the typical dating error of the RAT record along the MIS 7e averages ~1.2 kyr and comparably the Ejulve errors record averages ~2 kyr, both records strengthen enhanced humidity along this period. Speleothem records from the Austrian Alps (~0.3 kyr average errors) and Sardinia (~1.5 kyr average errors), also reflect warming or more humid conditions along the MIS 7e responding to changes in the North Atlantic realm (Spötl *et al.*,2008; Columbu *et al.*, 2019; Wendt *et al.*, 2020).

Similarly, long-term pollen records of the Mediterranean region show expansions of the arboreal vegetation coincident with precession minima because of warmer climate and greater water availability (Sánchez-Goñi *et al.*, 2008; Tzedakis *et al.*, 2006, 2009; Wagner *et al.*, 2019). In particular, the arboreal pollen percentages in the Tenaghi Philippon pollen record from Greece, in the eastern Mediterranean region, show an extraordinary resemblance with the precipitation variability recorded in the RAT Mg/Ca, where high arboreal pollen percentages are in line with enhanced precipitation (Fig. 3) (Tzedakis *et al.*, 2003, 2006). However, certain time discrepancies can be observed mostly during the end of the glacial MIS 10 and for the TIV and TIII.a. The Tenaghi Philippon age model relies on orbital tuning, assuming a constant lag of one thousand years in the orbital alignment, a circumstance that may account for certain discrepancies with the absolutely dated speleothem record. Aside from the age biases during deglaciations, both records exhibit proxy fluctuations associated with glacial/interglacial cycles as well as stadial/interstadial structures with a strong precession signal.

Precession has a major effect on the Mediterranean Sea due to its ability to disrupt the evaporation-precipitation balance of the sea basin. This influence has been documented through several proxy records that demonstrate modifications in oceanographic and sedimentary processes. For instance, marine sediment records close to the Strait of Gibraltar recorded changes in the Mediterranean Outflow Water strength (MOW), mainly driven by precession-controlled fluctuations in the Mediterranean hydrologic budget (Nichols *et al.,* 2020; Sierro *et al*., 2020), and marine sediments from the Balearic Sea documented carbonate cyclicities due to the control of the W Mediterranean cyclogenetic mechanisms (Ochoa *et al.,* 2018). The precession control on the African monsoon is well known, which indirectly also affected the eastern Mediterranean water properties, through river runoff along the North African coast, changing drastically the $\delta^{18}O_{sw}$ composition and allowing sapropel formations (Rohling *et al.,* 2014; Grant *et al*., 2016). Several studies highlight that the timing of enhanced summer monsoon corresponds with maximum Mediterranean autumn/winter storm track precipitation (Kutzbach *et al*., 2014; Toucanne *et al*., 2015; Wagner *et al*., 2019). The Mg/Ca-RAT record also reveals this concordance, where western Mediterranean enhanced precipitation, during interglacial/interstadial periods of precession minima, is consistently in line with higher summer monsoon intensities according to the Chinese speleothem records from Sanbao cave (Fig. 3) (Cheng *et al*., 2016).

3.2 Onset of glacial terminations

The newly obtained RAT records provide new constraints on the absolute age for glacial terminations TIV, TIII, and TIII.a based on the identification of meltwater release reflected in negative $\delta^{18}O$ excursions (Fig. 4A). Accordingly, the onset of TIV shows a first $\delta^{18}O$ depletion at 351±5 ka, followed by a larger depletion at 343±3 ka which likely reflecting the maximum rate of ice melting. This is consistent with a study based on volcanic interbed deposits of near-coastal aggradational successions in Italy (Fig. 4A horizontal purple bars), which provided independent ages for sea level rise by means of $^{40}Ar/^{39}Ar$ absolute dating (Marra *et al*., 2016, 2019). The onset of the TIII in the RAT speleothem is also in concordance with the sea-level rise observed in Italy, and the principal $\delta^{18}O$ negative anomaly occurred at 245±2 ka. This anomaly is comparable in magnitude to the TIV freshening. The TIII.a deglaciation is marked by the negative $\delta^{18}O$ anomaly centered at 227±1 ka (Fig. 4). This characteristic $\delta^{18}O$ feature of deglaciations is also recognized in the Mallorca speleothem (VALL 2) along the TV, although the high age uncertainties associated to the chronological limit of the U-Th technique preclude a precise date for the onset of this termination (appendix Fig. B1).

The peaks of maximum freshening for the three studied glacial terminations in RAT occurred during falling precession index and therefore consistent with the beginning of the summer insolation increases (Fig. 4B). In contrast, the obliquity phase is very variable among the three terminations. The TIV and TIII.a occurs during obliquity increase, while this parameter was decreasing through TIII. Hence, falling precession is the common orbital feature along the studied terminations, supporting the idea that precession appears more important than obliquity in predicting the onset of Late Pleistocene glacial terminations (Hobart *et al*., 2023).

Tzedakis *et al.*, 2017 proposed that the energy needed to force the glacial terminations also depends on the length and the intensity of the previous glacial period. The evaluation of the glacial conditions also reveals differences among the three studied terminations. Robust glacial conditions properly preconditioned the continental ice sheet volume before the TIV deglaciation. Lower precession amplitude, together with minimum obliquity through the full glacial conditions of the MIS 10, led to less caloric summer insolation before the TIV onset, strengthening the glacial maximum conditions. The caloric summer insolation is controlled by the combination of both, precession, and obliquity, and represents the amount of energy integrated over the caloric summer half of the year, certainly playing a causal role in the achievement of interglacial acmes (Milankovic, 1941; Tzedakis *et al.*, 2006). But it should also influence glacial attributes. The MIS 10 culminated with a maximum in the ice-sheet extent according to the benthic $\delta^{18}O$ record from the LR04 stack (Lisiecki and Raymo, 2005), but also observable in the more extreme positive glacial $\delta^{18}O$ in the $\delta^{18}O$ RAT record. Furthermore, IRDs were released continuously in the North Atlantic at the end of the MIS 10, contributing to freshwater inputs (Fig. 4C) (Barker *et al.*, 2015, 2019, 2021). These intense pre-deglacial conditions facilitated the early freshening phase at the onset of TIV and, may have reinforced the duration of the subsequent pronounced freshening and the relaxation time observed in the $\delta^{18}O$ RAT record. The maximum glacial conditions with noticeable IRD release did not present such a prominent ice volume maximum at the end of the MIS 8, neither in the benthic $\delta^{18}O$ nor in the RAT records. This glacial situation favored the shorter and less noticeable freshening of the TIII (Fig. 4C). The $\delta^{18}O$ RAT shows a similar freshening structure between TIII and TIII.a, despite TIII.a being an exceptional deglaciation because it does not proceed from full glacial conditions. Short cold stadial conditions, with less IRD release and accumulated ice volume, allowed anyway a strong response of the ice-sheet dynamics to the insolation rise probably due to the pronounced orbital changes through this deglaciation. Interestingly, the meltwater release of TIII.a culminated significantly before the summer caloric insolation maxima, reinforcing the exceptional character of this extra termination (Fig. 4C), while TIV and TIII are closer to their respective summer caloric insolation maxima. The extent of the studied freshenings is in line with AMOC weakening according to the Sanbao Chinese speleothems (Fig. 4D).

A comparison among the last five glacial terminations is presented in Figure 5. The studied terminations (TIV, TIII, and TIII.a) are directly compared with terminations TII and TI recorded in the $\delta^{18}O$ records of Cantabrian speleothems, from north Iberia Peninsula caves (Stoll *et al.*, 2015, 2022). The TII and TI also occurred in line with falling precession index. In the right panel,

all the records were centered at the first and most prominent $\delta^{18}O$ negative anomaly structure in order to compare their duration. The same exercise was performed with the isotopic measurements to observe the freshening magnitudes. This comparison underlines that TIII and TIII.a were those with less freshening magnitude while TIV was prominent. Unlike the benthic $\delta^{18}O$ records which feature a freshening and plateau at interglacial values, in the speleothem records the peak freshening marked by the negative $\delta^{18}O$ relaxes back to intermediate values. During TII, the period of most extreme negative $\delta^{18}O$ in North Iberia speleothems indicates fresher surface ocean $\delta^{18}O_{sw}$, highlighting the concentration of meltwater in the North Atlantic, and the relaxation has been interpreted to reflect the mixing of this meltwater anomaly throughout the global ocean as the rate of meltwater addition slows and the rate of overturning circulation strengthens (Stoll *et al.,* 2022). The RAT record suggests differences in the time required from the deglacial onset until the relaxation of these negative $\delta^{18}O$ anomalies, from very rapid (~5 kyr) during TIII.a, similar to the TI relaxation before the Bölling-Alleröd event, intermediate (~10 kyr) for TIII, similar to TII, and much slower (~20 kyr) for TIV (Fig. 5).
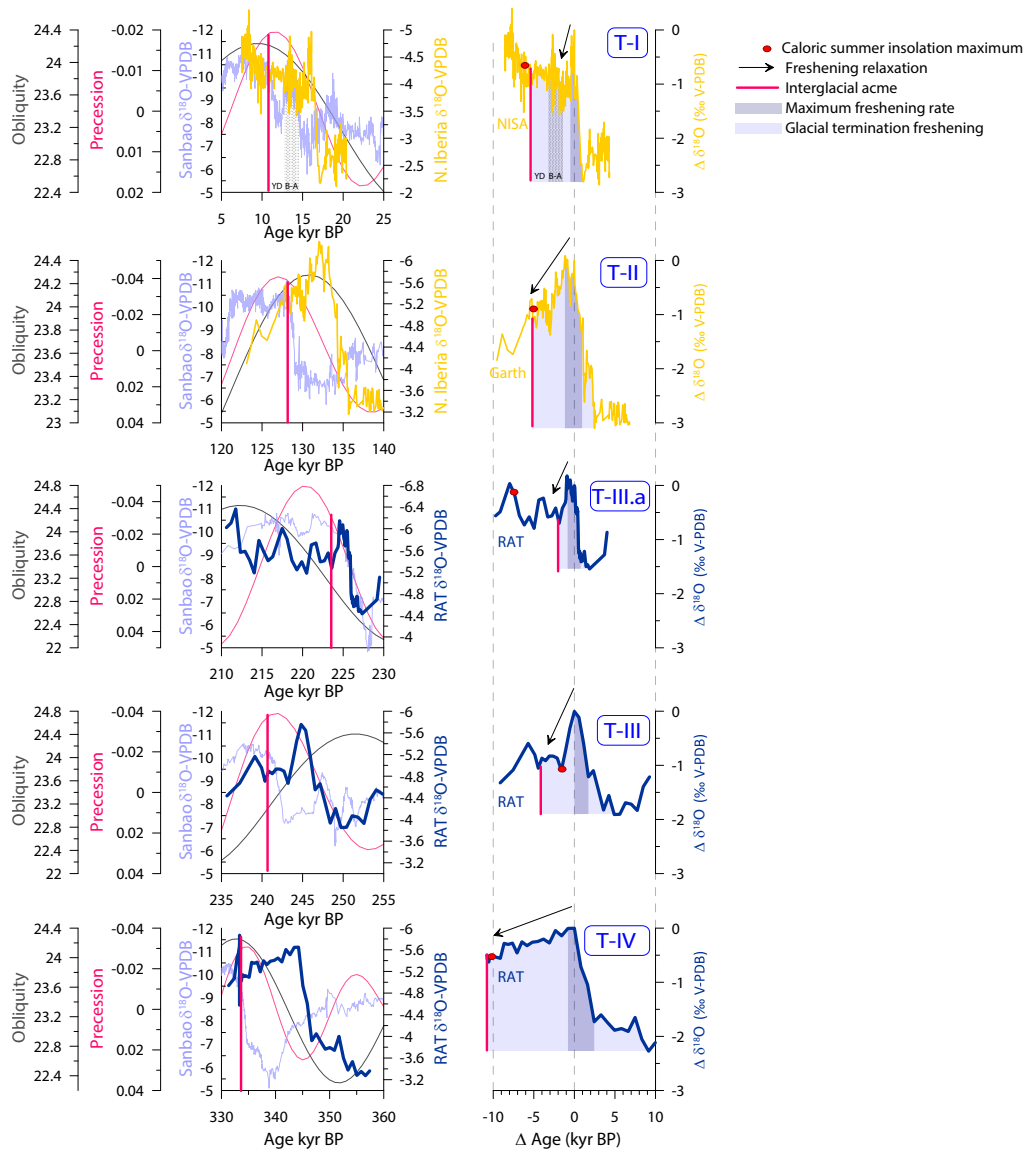
Figure 5: Comparison of the δ¹⁸O$_{speleo}$ records from the RAT speleothem and the North Iberian speleothems (Stoll *et al.*, 2022) along the last five glacial terminations. In the left panel, the speleothem records are plotted against the obliquity and precession parameters (Laskar, 2004). The onset of each interglacial acme is highlighted with a vertical pink line according to the Sanbao speleothem record (Cheng *et al.*, 2012, 2016), which considered the recovery of the Eastern Asian Summer Monsoon intensities as the end of the deglaciation. The right panel shows the duration and the magnitude of the δ¹⁸O freshening structures in Iberia using differential values in both the X and Y axes. The zero value corresponds to the first and most negative δ¹⁸O value of the main freshening structure of each termination. The black arrow underlines the freshening relaxation of the negative isotopic anomaly after the maximum freshening rate. The maximum summer caloric insolation after each glacial termination is also highlighted with a red circle. It is notable how different the positions of the summer caloric insolation maximum and precession minima are with respect to the freshening structure and the interglacial acme among the compared terminations.

3.2 Implications for Marine Chronologies

440   The RAT speleothem provides absolute chronologies for the deglacial time sequences in the western Mediterranean, which can be transferred to marine sequences that have proxies also sensitive to deglacial freshening. This is the case of the $\delta^{18}O_{planktic}$ data measured in *G. bulloides* from the ODP 977 site in the Alboran Sea, where their combined use with Mg/Ca derived temperatures has provided $\delta^{18}O_{sw}$ reconstructions that prove the arrival of north Atlantic freshening associates to the major melting phases of mostly the Fennoscandian ice sheets during TV, TIII.a, TII and TI (Azibeiro *et al.,* 2021; González-Mora *et*

445   *al.,* 2008; Jiménez-Amat and Zahn, 2015; Torner *et al.*, 2019; Stoll *et al.*, 2022). These studies conducted at the ODP 977 site indicate that the timing and magnitude of the main negative $\delta^{18}O_{sw}$ shift are synchronous with $\delta^{18}O_{planktic}$ changes at glacial terminations, suggesting that the freshwater signal may have a dominant influence on the $\delta^{18}O_{planktic}$ variability (appendix Fig. E1). Moreover, the amplitude between the deglacial anomalies of the $\delta^{18}O_{planktic}$ record in the ODP 977 and the $\delta^{18}O$ RAT records are similar for the three studied terminations. Hence, the new $\delta^{18}O_{planktic}$ data for TIV, TIII, and TIII.a provide an

450   exceptional base to tune the millennial-scale features of the marine record to our dated $\delta^{18}O$ RAT record, achieving an orbitally independent chronology. Therefore, the more negative $\delta^{18}O_{planktic}$ structures have been used to align the chronology with the $\delta^{18}O$ negative anomalies of RAT during the glacial terminations. The resulting ODP 977 age model is shown in Appendix Figure F1, where the tie points used by the alignment can be observed. Freshening due to ice-melting is notable in the $\delta^{18}O_{planktic}$ ODP 977 signature and the resemblance with the $\delta^{18}O$ RAT record is remarkable during glacial terminations (Fig. 4E). This

455   new ODP 977 chronology is further applied to records from the Atlantic Iberian Margin (MD01-2444), also containing deglacial negative $\delta^{18}O_{planktic}$ anomalies (Fig. 4E) (Tzedakis *et al.*, 2018; Hodell *et al.*, 2013). Several tie points have also been used to tune the MD01-2444 in the base of the most relevant structures (appendix Fig. F1). All the correlations among the tuned records were estimated by linear interpolation using the Analyseries Software package (Paillard *et al.*, 1996). Particularly, the adjusted TIV exhibits a temporal discrepancy of ~7.4 kyr compared to the established chronology, and the

460   mean age uncertainty of the RAT speleothem throughout this termination is less than this difference, approximately ±3.4 kyr. In contrast, the TIII aligns well with previously published chronologies due to a minor time discrepancy, approximately ~3 kyr, similar to the RAT average age uncertainty of ±1.5 kyr. In the case of TIII.a, the chronological discrepancy is even more significant, reaching ~11 kyr, with average errors of the RAT estimated to be around ±1 kyr. Hence, this exercise reveals significant time discrepancies, particularly for TIV and TIII.a, and exposes that marine chronologies remain unconstrained

465   mostly for glacial termination onsets. This study supports the idea that millennial-scale variability could strongly influence climate variation along deglaciations (Barker *et al.*, 2021) and highlights that the distinctive characteristic of each glacial termination should be seriously considered to tune the marine chronologies. In addition, it exposes the power of the RAT speleothem as an excellent example to evaluate the time sequences of TIV and TIII.a, and encourages the revision of the marine chronologies to clarify glacial termination dynamics independently of the orbital bond.

4 Conclusions

Geochemical proxies in the speleothem RAT reveal alternating dry glacial conditions and wet interglacial conditions in the western Mediterranean region from MIS 11 to MIS 7. Deglaciations were systematically initiated with major ocean freshening events in the North Atlantic, recorded as negative $\delta^{18}O$ anomalies in the speleothem, and in parallel with extreme arid conditions in the western Mediterranean region according to the Mg/Ca. This study provides further evidence that falling precession was the major orbital trigger for glacial terminations and constrains the deglacial time sequences of each studied glacial termination. Despite the common features, the three deglaciations present differences in terms of magnitude, intensity, and duration. The dissimilarities along the preceding glacial conditions also contributed to these distinctive features. TIV was slower, longer, and more intense than TIII and TIII.a. The RAT record provides an absolute chronology for the intense meltwater release events that initiated the glacial terminations, but also for the maximum freshening of each deglaciation: TIV onset at 351±5 ka BP and maximum freshening peak at 343±3 ka, the TIII onset at 251±3 ka and the maximum freshening peak at 245±2 ka, and finally the TIII.a onset at 229±2 ka BP and the maximum freshening peak at 227±1 ka. The newly achieved chronology indicates that revision is needed to the most common marine chronologies, mostly for TIV and TIII.a, which are based on orbital tuning. These discrepancies and the role of millennial-scale variability associated with the onset of glacial terminations suggest that a standard orbital tuning of marine sequences will often not yield a robust chronology. The RAT speleothem provides for the very first time the possibility to validate and improve the accuracy of North Atlantic and Western Mediterranean marine chronologies by independent absolute dating.

5 Appendices

Appendix A) U/Th laboratory procedure

Speleothem carbonate sample powders were dissolved in 7N HNO_3 and spiked with an in-house solution with known ^{233}U, ^{236}U, and ^{229}Th concentrations. After that, a few drops of concentrated $HClO_4$ were added to attack and remove organic matter. After one hour of refluxing, the samples were completely dried and re-dissolved in 2N HCl. The U and Th were isolated from Ca and several trace elements by means of an iron co-precipitation. Then, 1-2 drops of $FeCl_2$ were added, and several NH_4OH drops were added later to induce the Fe precipitation together with U and Th. Afterward, samples were centrifuged and rinsed with super-clean water three times while the overlying liquid was removed. In order to separate Fe from U and Th, iron samples were dissolved and loaded in anion exchange resin columns. While Fe was removed with 7N HNO_3, Th was collected with 6N HCl and separated from U, which was recovered ultimately with super-clean water. Each pair of samples were dried and dissolved in a low-concentrated nitric acid and analyzed by means of multi-collector inductively coupled plasma mass spectrometry at the University of Minnesota and the Xi'an Jiaotong University. Results and dating errors of the RAT and VALL 2 speleothems are found in Table A1.

Sample number	Depth (cm)	Sample Label	^{238}U (ppb)	^{232}Th (ppt)	^{230}Th / ^{232}Th (atomic x10^{-6})	δ^{234}U* (measured)	^{230}Th / ^{238}U (activity)	^{230}Th Age (yr) (uncorrected)	^{230}Th Age (yr) (corrected)	δ^{234}U$_{initial}$** (corrected)	^{230}Th Age (yr BP)*** (corrected)
1	0.75	RAT_A	186.0 ±0.2	1697 ±34	3951 ±79	1249.1 ±2.5	2.1858 ±0.0039	210673 ±1087	210591 ±1088	2263 ±8	210525 ±1088
2	7.25	RAT_A.1	125.6 ±0.1	1179 ±24	3947 ±79	1246.2 ±2.2	2.2458 ±0.0033	226066 ±1054	225984 ±1055	2358 ±8	225918 ±1055
3	7.25	RAT-2.75	177.3 ±0.1	106 ±2	62119 ±1434	1257.5 ±1.9	2.2584 ±0.0033	226101 ±993	226095 ±993	2380 ±8	226024 ±993
4	8.5	RAT_B	118.7 ±0.1	645 ±13	6804 ±137	1235.1 ±2.7	2.2415 ±0.0044	228149 ±1397	228102 ±1397	2351 ±11	228036 ±1397
5	9.75	RAT_B.1	83.8 ±0.1	1188 ±24	2542 ±51	1200.3 ±2.3	2.1862 ±0.0052	223677 ±1510	223550 ±1511	2256 ±11	223484 ±1511
6	13.5	RAT_B.2	85.7 ±0.1	1269 ±25	2389 ±48	1135.8 ±2.1	2.1465 ±0.0037	232313 ±1265	232178 ±1267	2187 ±9	232112 ±1267
7	14	RAT 2	85.5 ±0.1	284 ±6	10808 ±221	1156.0 ±1.9	2.1804 ±0.0031	235607 ±1093	235576 ±1093	2247 ±8	235505 ±1093
8	15	RAT c	54.6 ±0.1	584 ±12	3312.0 ±66.6	1120.2 ±2.1	2.1475 ±0.0035	237779 ±1277	237680 ±1278	2191 ±8.9	237616 ±1278
9	15.25	RAT 3.25	70.9 ±0.1	1169 ±23	2108 ±42	1085.7 ±1.6	2.1074 ±0.0036	237367 ±1258	237213 ±1261	2121 ±8	237142 ±1261
10	15.5	RAT_C.1	76.1 ±0.1	4946 ±99	519 ±10	1009.5 ±2.0	2.0490 ±0.0038	246517 ±1518	245888 ±1574	2021 ±10	245822 ±1574
11	16	RAT_D	75.3 ±0.1	2113 ±42	1159 ±23	925.9 ±2.0	1.9725 ±0.0033	253671 ±1568	253388 ±1578	1893 ±9	253326 ±1578
12	16.5	RAT 4.5	56.9 ±0.0	457 ±9	4187 ±85	926.5 ±1.7	2.0405 ±0.0039	282375 ±2087	282297 ±2087	2055 ±13	282226 ±2087
13	17	RAT 5	67.7 ±0.1	75 ±2	29556 ±732	887.3 ±1.7	1.9982 ±0.0034	284836 ±1946	284824 ±1946	1982 ±12	284753 ±1946
14	17.7	RAT 5.7	71.3 ±0.1	110 ±2	20978 ±466	859.2 ±1.6	1.9700 ±0.0036	287778 ±2109	287761 ±2109	1935 ±12	287690 ±2109
15	18.25	RAT_E	78.5 ±0.1	654 ±13	3843 ±77	834.4 ±2.0	1.9399 ±0.0038	287767 ±2405	287682 ±2404	1879 ±14	287620 ±2404
16	20	RAT_E.1	90.0 ±0.1	445 ±9	6121 ±124	738.5 ±2.2	1.8340 ±0.0036	293865 ±2657	293810 ±2656	1692 ±14	293744 ±2656
17	23	RAT_F	94.2 ±0.1	657 ±13	4069 ±82	636.2 ±1.8	1.7211 ±0.0034	301956 ±2809	301874 ±2808	1491 ±13	301812 ±2808
18	24	RAT 12	79.5 ±0.1	28 ±1	77872 ±3369	571.6 ±1.4	1.6549 ±0.0027	312266 ±2597	312260 ±2597	1380 ±13	312189 ±2597
19	26	RAT_F.1	80.5 ±0.1	55 ±2	38662 ±1081	528.9 ±1.9	1.6075 ±0.0024	317242 ±3246	317232 ±3246	1295 ±13	317166 ±3246
20	28	RAT_G	96.1 ±0.1	230 ±5	10923 ±221	515.8 ±1.9	1.5882 ±0.0034	314689 ±3633	314657 ±3632	1253 ±14	314595 ±3632
21	28.75	RAT_H	87.6 ±0.1	686 ±14	3275 ±66	486.5 ±1.7	1.5556 ±0.0035	318254 ±3778	318148 ±3776	1194 ±13	318086 ±3776
22	29.5	RAT_H.1	103.9 ±0.1	172 ±4	15358 ±318	476.0 ±2.0	1.5440 ±0.0034	319752 ±3689	319729 ±3689	1173 ±13	319663 ±3689
23	32	RAT_H.2	63.9 ±0.0	144 ±3	11459 ±245	485.3 ±1.7	1.5627 ±0.0030	326523 ±3661	326492 ±3661	1219 ±13	326426 ±3661
24	32.75	RAT_I	89.9 ±0.1	153 ±3	15552 ±315	520.6 ±1.8	1.6073 ±0.0039	326426 ±4204	326404 ±4203	1308 ±16	326342 ±4203
25	34	RAT_I.1	72.7 ±0.1	217 ±4	9021 ±186	535.3 ±1.9	1.6372 ±0.0033	337484 ±4138	337446 ±4137	1387 ±17	337380 ±4137
26	35	RAT_J	81.5 ±0.1	162 ±3	13893 ±281	573.2 ±1.8	1.6805 ±0.0036	332647 ±3944	332622 ±3943	1465 ±17	332560 ±3943
27	35.75	RAT 23.75	81.9 ±0.1	100 ±2	22796 ±523	576.1 ±1.4	1.6865 ±0.0030	334834 ±3324	334818 ±3323	1482 ±14	334747 ±3323
28	36.6	RAT 24.6	90.5 ±0.1	470 ±10	5671 ±115	655.1 ±1.6	1.7878 ±0.0027	335551 ±2982	335493 ±2981	1688 ±15	335422 ±2981
29	36.75	RAT_J.1	80.7 ±0.1	195 ±4	11499 ±240	573.5 ±1.8	1.6833 ±0.0034	334990 ±3912	334960 ±3911	1476 ±17	334894 ±3911
30	37	RAT 25	99.5 ±0.1	428 ±9	7265 ±147	731.9 ±1.5	1.8963 ±0.0030	344621 ±3138	344576 ±3137	1935 ±18	344505 ±3137
31	37.25	RAT_J.2	85.1 ±0.1	572 ±12	5019 ±102	838.0 ±2.2	2.0452 ±0.0041	355336 ±4289	355275 ±4288	2284 ±28	355209 ±4288
32	37.5	RAT 25.5	100.9 ±0.1	556 ±11	6141 ±124	845.7 ±1.6	2.0529 ±0.0035	353380 ±3159	353330 ±3158	2292 ±21	353259 ±3158
33	38.5	RAT_J.3	122.2 ±0.1	113 ±2	35121 ±759	768.4 ±1.8	1.9654 ±0.0028	365001 ±3564	364990 ±3564	2152 ±22	364924 ±3564
34	39	RAT 27	134.4 ±0.1	59 ±2	71303 ±1884	712.5 ±1.5	1.9010 ±0.0031	373880 ±4055	373874 ±4055	2047 ±24	373803 ±4055
35	40.1	RAT_J.4	151.9 ±0.2	59 ±2	80965 ±2468	716.0 ±1.9	1.9038 ±0.0036	372020 ±4716	372014 ±4716	2046 ±28	371948 ±4716
36	45	RAT_J.5	146.9 ±0.2	53 ±2	86817 ±2581	723.2 ±2.0	1.9102 ±0.0033	368865 ±4477	368860 ±4477	2048 ±27	368794 ±4477
37	47	RAT_J.6	118.5 ±0.1	45 ±1	81924 ±2440	716.5 ±2.1	1.9001 ±0.0035	367292 ±4708	367287 ±4708	2020 ±28	367221 ±4708
38	48.5	RAT 36.5	117.5 ±0.1	183 ±4	20120 ±425	712.1 ±1.6	1.9027 ±0.0041	376488 ±5495	376472 ±5494	2060 ±32	376401 ±5494
39	50	RAT_J.7	92.8 ±0.1	52 ±2	55752 ±1711	709.6 ±2.5	1.9067 ±0.0049	384890 ±7090	384883 ±7090	2103 ±43	384817 ±7090
40	50.7	RAT 38.7	70.3 ±0.0	41 ±1	53378 ±1862	709.7 ±1.9	1.9042 ±0.0037	381728 ±5194	381721 ±5194	2084 ±31	381650 ±5194
41	51.5	RAT k	86.0 ±0.1	258 ±5	10410 ±211	707.5 ±2.0	1.8948 ±0.0033	374408 ±4678	374378 ±4677	2035 ±27	374314 ±4677

^{230}Th dating results. The error is 2σ error.

Sample number	Depth (cm)	Sample Number	^{238}U (ppb)	^{232}Th (ppt)	^{230}Th / ^{232}Th (atomic x10^{-6})	δ^{234}U* (measured)	^{230}Th / ^{238}U (activity)	^{230}Th Age (yr) (uncorrected)	^{230}Th Age (yr) (corrected)	δ^{234}U$_{initial}$** (corrected)	^{230}Th Age (yr BP)*** (corrected)
1	0.2	VALL2_0.2	1294.6 ±3.1	41 ±1	452066 ±15597	108.8 ±2.0	0.8697 ±0.0025	159998 ±1252	159997 ±1252	171 ±3	159931 ±1252
2	1.8	VALL2_Top	342.8 ±0.6	12 ±0	485542 ±11926	39.1 ±1.7	1.0199 ±0.0030	377308 ±11561	377304 ±11561	113 ±6	377242 ±11561
3	4.3	VALL2_4.3	289.3 ±0.4	28 ±1	170650 ±5044	32.0 ±1.5	1.0152 ±0.0018	392841 ±9902	392835 ±9902	97 ±5	392769 ±9902
4	5.5	VALL2_5.5	334.2 ±0.5	4 ±1	1295999 ±278065	28.8 ±1.7	1.0207 ±0.0017	436721 ±15916	436716 ±15915	99 ±7	436650 ±15915
5	7	VALL2_7	315.9 ±0.4	23 ±1	230927 ±13011	31.1 ±1.5	1.0199 ±0.0021	416922 ±13354	416916 ±13353	101 ±6	416850 ±13353
6	7.6	VALL2_7.6	284.5 ±0.4	10 ±1	503033 ±40961	35.3 ±1.7	1.0281 ±0.0018	429141 ±14893	429136 ±14893	118 ±8	429070 ±14893
7	8.1	VALL2_8.1	372.4 ±0.6	19 ±1	334429 ±20523	40.4 ±1.8	1.0395 ±0.0020	454126 ±19373	454119 ±19372	145 ±10	454053 ±19372
8	8.6	VALL2_8.6	246.9 ±0.3	36 ±1	118137 ±4037	39.7 ±1.5	1.0416 ±0.0020	474894 ±21176	474883 ±21175	151 ±11	474817 ±21175
9	9	VALL2_9	770.8 ±1.8	10 ±1	1321617 ±104976	31.0 ±2.0	1.0321 ±0.0026	494581 ±34732	494572 ±34730	125 ±15	494506 ±34730
10	12	VALL2_12	811.2 ±2.3	56 ±2	247280 ±6969	25.2 ±2.6	1.0284 ±0.0033	540121 ±73096	540107 ±73086	117 ±28	540041 ±73086
11	15.6	VALL2_15.6	211.6 ±0.2	24 ±1	148538 ±6320	25.4 ±1.5	1.0246 ±0.0019	495996 ±26282	495984 ±26280	103 ±10	495918 ±26280
12	18	VALL2_18	335.5 ±0.4	29 ±1	194361 ±7398	25.1 ±1.5	1.0260 ±0.0020	514267 ±32267	514255 ±32264	107 ±12	514189 ±32264
13	20.3	VALL2_Bottom	349 ±1	11 ±1	549205.7 ±32644.0	23.9 ±1.5	1.0251 ±0.0033	523624 ±48562	523612 ±48557	105 ±16	523550 ±48557

U decay constants: $\lambda_{238} = 1.55125 \times 10^{-10}$ (Jaffey et al., 1971) and $\lambda_{234} = 2.82206 \times 10^{-6}$ (Cheng et al., 2013). Th decay constant: $\lambda_{230} = 9.1705 \times 10^{-6}$ (Cheng et al., 2013).

*δ^{234}U = ([^{234}U/^{238}U]$_{activity}$ – 1)x1000. ** δ^{234}U$_{initial}$ was calculated based on ^{230}Th age (T), i.e., δ^{234}U$_{initial}$ = δ^{234}U$_{measured}$ x e$^{\lambda_{234} \times T}$.

Corrected ^{230}Th ages assume the initial ^{230}Th/^{232}Th atomic ratio of 4.4 ±2.2 x10^{-6}. Those are the values for a material at secular equilibrium, with the bulk earth ^{232}Th/^{238}U value of 3.8. The errors are arbitrarily assumed to be 50%.

***B.P. stands for "Before Present" where the "Present" is defined as the year 1950 A.D.

500

Table A1: U/Th dates from RAT and VAll 2 speleothems
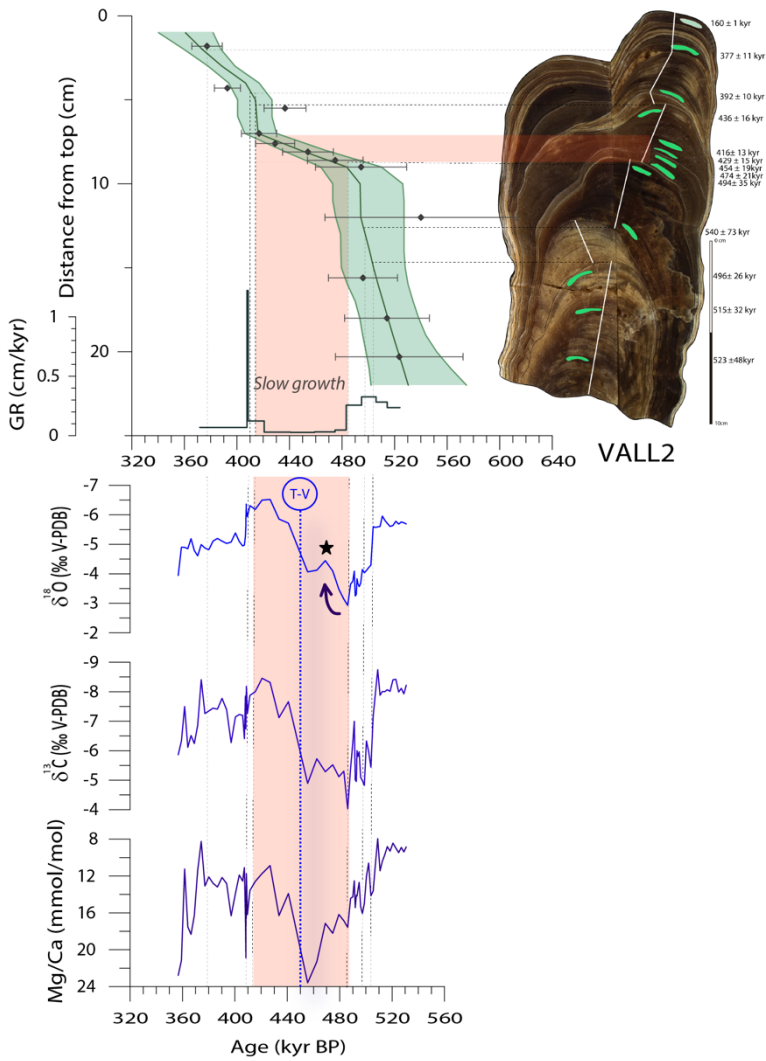
Figure B1: VALL 2 speleothem age model acquired by StalAge (dark blue line) and the original U/Th dates (dark blue dots), plotted with the associated errors (error bars and green area). The VALL2 growth rates are shown in dark green. On the right, there is the speleothem image with the position of the sampled radiometric dates used for the age model and the growth axis path used for the geochemical analyses (white line). In the lower panel the δ18O, δ13C, and Mg/Ca results with reversal axes. The pink bar highlights a slow growth rate and the dashed grey line points to major color and growth axis direction changes of the speleothem.
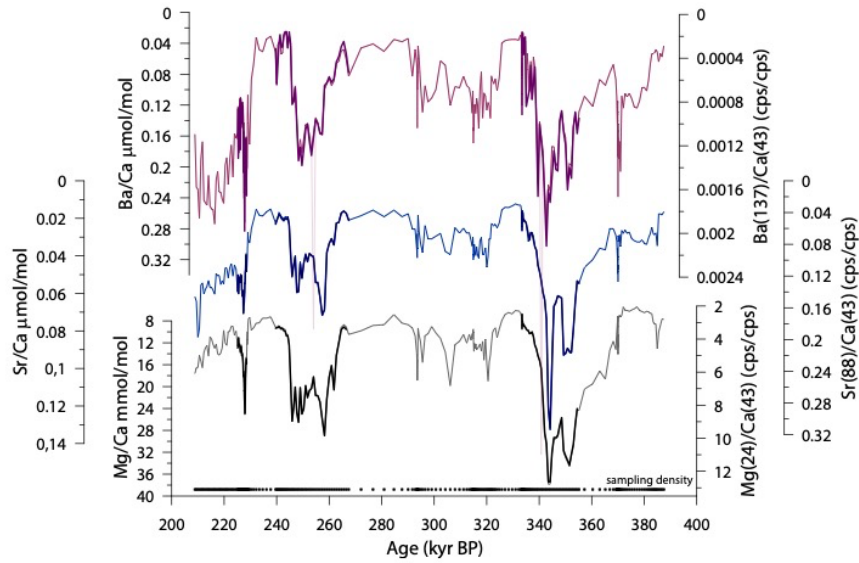
Figure C1: RAT Mg/Ca ratios compared with Sr/Ca and Ba/Ca ratios in both, counts per second, right axes, and the calculated mmol/mol and μmol/mol values at left axes.
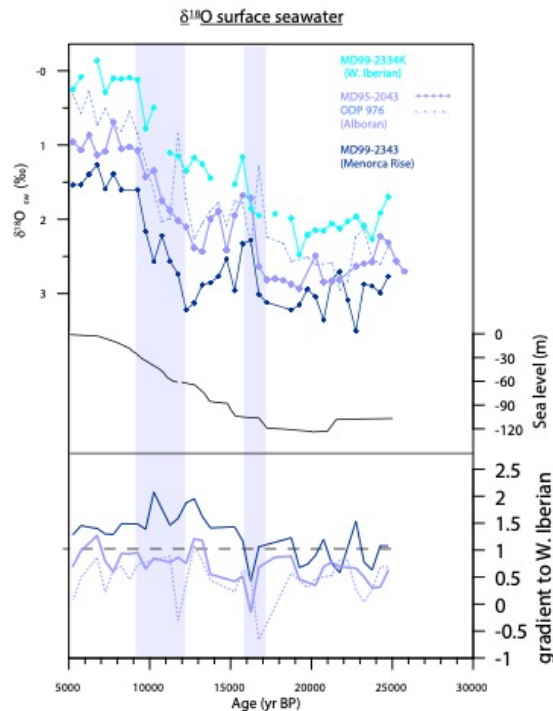
Figure D1: Transmission of the seawater isotopic signal from the N. Atlantic to the Mediterranean Sea along the TI modified from Stoll *et al.*, (2022). The $\delta^{18}O_{sw}$ values from paired Mg/Ca and $\delta^{18}O_{plank}$ decline along the deglaciation, with two well-recognized major freshening steps, one abrupt around 16 ka, and the other more gradual from about 12 to 10 ka (blue vertical bars). These freshenings were recorded synchronously and with a similar magnitude in different sediment records from three different locations. The core

MD99-2334K from the western Iberian margin in the N. Atlantic (Skinner *et al.,* 2006), two sediment cores from the Alboran Sea in the western Mediterranean (Català *et al.,* 2019), both close to the ODP 977 site. And the MD99-2343 core from the Balearic Sea (Català *et al.,* 2019). Sea level rise from Lambeck *et al*., (2014). In the bottom panel, the gradient of the isotopic signal between the Alboran or the Balearic Sea against the W. Iberian record shows the characteristic enrichment of the seawater throughout the Mediterranean Sea, with probably higher evaporative processes in the Menorca rise leading to even heavier values in this basin.
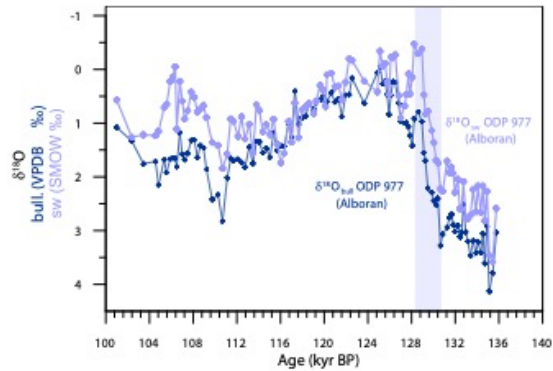
Figure E1: Comparison between the *G. bulloides* $\delta^{18}O_{plank}$ of the ODP 977 site and the $\delta^{18}O_{sw}$ signal, obtained by removing the temperature effect using the derived SST-Mg/Ca also measured in *G. bulloides* of the same sediment core along glacial termination II (Torner *et al*., 2019). The maximum rate of freshening along deglaciation coincides in both records as rapid negative $\delta^{18}O$ anomalies and is highlighted by a blue bar.
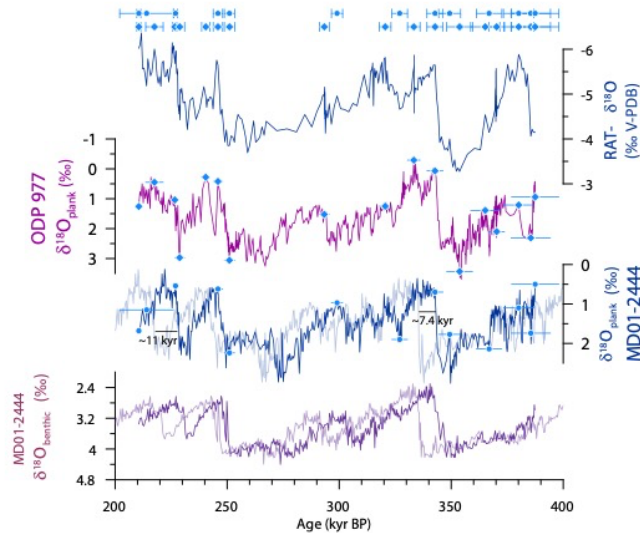
Figure F1: Marine sediment tuning strategy using the RAT age model. At the top, blue circles and diamonds indicate the tie points used for chronological alignment with the speleothem errors associated according to the RAT $\delta^{18}O$ record. The ODP 977 $\delta^{18}O$ record on the RAT speleothem chronology is in the middle. At the bottom, the MD01-2444 planktic and benthic $\delta^{18}O$ records on the RAT speleothem chronology and with the original chronology in light color (Tzedakis *et al.*, 2018).

6 Data availability

Upon acceptance, RAT data will be presented for inclusion in the subsequent version of SISAL.

7 Author contributions

JT and IC designed and conceptualized the study. JT conducted measurements and analyzed the results. AM and HS
provided scientific guidance. JJF coordinated the fieldwork in Mallorca. HC and RLE provided laboratory facilities and
funding for U/Th measurements. FJS and JOG provided resources and interpretation of marine core ODP 977. JT was
responsible for writing the original draft, while all authors contributed to the discussion and interpretations of the final
manuscript.

8 Competing interests

The authors declare that they have no conflict of interest

9 Acknowledgements

This research was financially supported by the OPERA project (CTM2013-48639-C2-1-R), the CHIMERA project
(CTM2016-75411-R), the TRANSMOW project (PID2019-105523RB-I00), and the PID2020-112720GB-I00 project of the
Agencia Estatal de Investgación of the Ministerio de Ciencia e Innovación. Also has received funding from the European
Research Council (ERC) Consolidation Grant (No. 683237-TIMED). IC thanks the ICREA- Academia program from the
Generalitat de Catalunya. JT and IC acknowledge the financial support by a Catalan Government Grups de Recerca Consolidats
grant (2021 SGR 01195). The authors are grateful to M. Romero and J. Perona from CCiTUB for laboratory support. Thanks
to M. Cerdà for his collaboration with the artworks of the maps. Thanks to the members from the Societat Espeleològica Balear
for their field support during cave sampling

10 References

Azibeiro, L. A., Sierro, F. J., Capotondi, L., Lirer, F., Andersen, N., González-Lanchas, A., Alonso-Garcia, M., Flores, J. A.,
Cortina, A., Grimalt, J. O., Martrat, B., and Cacho, I.: Meltwater flux from northern ice-sheets to the mediterranean during
MIS 12, Quat Sci Rev, 268, https://doi.org/10.1016/j.quascirev.2021.107108, 2021.

Bar-Matthews, M., Ayalon, A., Kaufman, A., and Wasserburg, G.: The Eastern Mediterranean paleoclimate as a reflection of

560 region events:, Soreq Cave, Isr. Earth Planet. Sci. Lett., 166, 85–95, https://doi.org/10.1016/S0012-821X(98)00275-1, 1999.

Bar-Matthews, M., Ayalon, A., and Kaufman, A.: Timing and hydrological conditions of Sapropel events in the Eastern Mediterranean, as evident from speleothems, Soreq (Barker, 2021)2541(99)00232-6, 2000.

Bar-Matthews, M., Ayalon, A., Gilmour, M., Matthews, A., and Hawkesworth, C. J.: Sea – land oxygen isotopic relationships from planktonic foraminifera and speleothems in the Eastern Mediterranean region and their implication for paleorainfall

565 during interglacial intervals, 67, 3181–3199, 2003.

Barker, S., Barker, S., Knorr, G., Edwards, R. L., Parrenin, F., Putnam, A. E., Skinner, L. C., Wolff, E., and Ziegler, M.: 800,000 Years of abrupt climate variability, Science, 334, 0–5, https://doi.org/10.1126/science.1203580, 2011.

Barker, S., Chen, J., Gong, X., Jonkers, L., Knorr, G., and Thornalley, D.: Icebergs not the trigger for North Atlantic cold events, Nature, 520, 333–336, https://doi.org/10.1038/nature14330, 2015.

570 Barker, S., Knorr, G., Conn, S., Lordsmith, S., and Newman, D.: Early Interglacial Legacy of Deglacial Climate Instability Paleoceanography and Paleoclimatology, 2, 1455–1475, https://doi.org/10.1029/2019PA003661, 2019.

Barker, S. and Knorr G., Millennial scale feedbacks determine the shape and rapidity of glacial termination, Nat. Commun., 14, https://doi.org/10.1038/s41467-021-22388-6, 2021.

Bartolomé, M., Moreno, A., Sancho, C., Stoll, H. M., Cacho, I., Spötl, C., Belmonte, Á., Edwards, R. L., Cheng, H., and

575 Hellstrom, J. C.: Hydrological change in Southern Europe responding to increasing North Atlantic overturning during Greenland Stadial 1, Proc. Natl. Acad. Sci., 112, 6568–6572, https://doi.org/10.1073/pnas.1503990112, 2015.

Boers, N. Observation-based early-warning signals for a collapse of the Atlantic Meridional Overturning Circulation. Nat. Clim. Chang. 11, 680–688. https://doi.org/10.1038/s41558-021-01097-4, 2021.

Cacho, I., Grimalt, J. O., Pelejero, C., Canals, M., Sierro, F. J., Flores, J. A., and Shackleton, N.: Dansgaard-Oeschger and

580 Heinrich event imprints in Alboran Sea paleotemperatures, Paleoceanography, 14, 698–705, https://doi.org/10.1029/1999PA900044, 1999.

Cai, Y., Fung, I. Y., Edwards, R. L., An, Z., Cheng, H., Lee, J., Tan, L., and Shen, C. C., Wang, X., Day, J. A., Zhou, W., Kelly, M. J., and Chiang, J. C. H.: Variability of stalagmite-inferred Indian monsoon precipitation over the past 252 , 000 y, Proc. Natl. Acad. Sci. U. S. A., 11210, 2954–2959, https://doi.org/10.1073/pnas.1424035112, 2015.

585 Català, A., Cacho, I., Frigola, J., Pena, L. D. & Lirer, F. Holocene hydrography evolution in the Alboran Sea: a multi-record and multi-proxy comparison. Climate of the Past 15, 927-942, 2019.

Cheng H., Edwards R. L., Wang Y., Kong X., Ming Y., Kelly M. J., Wang X. and Gallup C. D.:. A penultimate glacial monsoon record from Hulu Cave and two-phase glacial terminations. Geology 34, 217–220, 2006.

Cheng, H., Edwards, R. L., Broecker, W. S., Denton, G. H., Kong, X., Wang, Y., Zhang, R., and Wang, X.: Ice Age

590 Terminations, Science, 248-252, 326, 2009.

Cheng, H., Spötl, C., Breitenbach, S. F. M., Sinha, A., Wassenburg, J. A., Jochum, K. P., Scholz, D., Li, X., Yi, L., Peng, Y., Lv, Y., Zhang, P., Votintseva, A., Loginov, V., Ning, Y., Kathayat, G., and Edwards, R. L.: Climate variations of Central Asia on orbital to millennial timescales, Sci. Rep., 5, 1–11, https://doi.org/10.1038/srep36975, 2016.

595 Clark, P. U., Shakun, J. D., Baker, P. A., Bartlein, P. J., Brewer, S., Brook, E., Carlson, A. E., Cheng, H., Kaufman, D. S., Liu, Z., Marchitto, T. M., Mix, A. C., Morrill, C., Otto-Bliesner, B. L., Pahnke, K., Russell, J. M., Whitlock, C., Adkins, J. F., Blois, J. L., Clark, J., Colman, S. M., Curry, W. B., Flower, B. P., He, F., Johnson, T. C., Lynch-Stieglitz, J., Markgraf, V., McManus, J., Mitrovica, J. X., Moreno, P. I., and Williams, J. W.: Global climate evolution during the last deglaciation, Proc Natl Acad Sci U S A, 109, https://doi.org/10.1073/pnas.1116619109, 2012

Columbu, A., Spötl, C., De Waele, J., Yu, T. L., Shen, C. C., and Gázquez, F.: A long record of MIS 7 and MIS 5 climate and
600 environment from a western Mediterranean speleothem (SW Sardinia, Italy), Quat. Sci. Rev., 220, 230–243, https://doi.org/10.1016/j.quascirev.2019.07.023, 2019.

Coplen, T. B.: New guidelines for reporting stable hydrogen, carbon, and oxygen isotope-ratio data, Geochim. Cosmochim. Acta, 60, 3359–3360, https://doi.org/10.1016/0016-7037(96)00263-3, 1996.

Cruz F. W., Burns S. J., Karmann I., Sharp W. D., Vuille M., Cardoso A. O., Ferrari J. A., Silva Dias P. L. and Viana O.,
605 Insolation-driven changes in atmospheric circulation over the past 116,000 years in subtropical Brazil. Nature, 434, 63–66, 2005.

Cruz F. W., Vuille M., Burns S. J., Wang X., Cheng H., Werner M., Lawrence Edwards R., Karmann I., Auler A. S. and Nguyen H., Orbitally driven east–west antiphasing of South American precipitation. Nat. Geosci. 2, 210– 214, 2009.

Dorale, J. A., Onac, B. P., Fornós, J. J., Ginés, J., Ginés, A., Tuccimei, P., and Peate, D. W.: Sea-level highstand 81, 000 years
610 ago in mallorca, Science, 327, 860–863, https://doi.org/10.1126/science.1181725, 2010.

Drysdale, R. N., Zanchetta, G., Hellstrom, J. C., Fallick, A. E., Zhao, J. X., Isola, I., & Bruschi, G., Palaeoclimatic implications of the growth history and stable isotope $\delta^{18}O$ and $\delta^{13}C$. Geochemistry of a Middle to Late Pleistocene stalagmite from central-western Italy. Earth and Planetary Science Letters, 2273–4, 215–229. https://doi.org/10.1016/j.epsl.2004.09.010, 2004.

Drysdale, R. N. Hellstrom, J. C., Zanchetta, G., Fallick, A. E., Sánchez-Goñi, M. F., Couchoud, I.,. Evidence for obliquity
615 forcing of glacial termination II. Science, 3255947., pp.1527–1531. doi: 10.1126/science.1170371, 2009.

Dumitru, O. A., Forray, F. L., Fornós, J. J., Ersek, V., Onac, B. P., Water isotopic variability in Mallorca: a path to understanding past changes in hydroclimate. Hydrol. Process. 31, 104–116. doi:10.1002/hyp.10978, 2017.

Dumitru, O. A., Onac, B. P., Polyak, V. J., Wynn, J. G., Asmerom, Y., Fornós, J. J., Climate variability in the western Mediterranean between 121 and 67 ka derived from a Mallorcan speleothem record. Palaeogeogr. Palaeoclimatol. Palaeoecol.
620 506, 128–138. doi:10.1016/j.palaeo.2018.06.028, 2018.

Fairchild, I.J., Borsato, A., Tooth, A.F., Frisia, S., Hawkesworth, C.J., Huang, Y., McDermott, F., Spiro, B., Controls on trace element Sr-Mg. compositions of carbonate cave waters: Implications for speleothem climatic records. Chem. Geol. 166, 255–269. doi:10.1016/S0009-254199.00216-8, 2000.

García-Alix, A. Jon Camuera, Maria José Ramos-Román, Jaime L-Toney, Dirk Sachse, Enno Schefub, Gonzalo Jimenez-
Moreno, Francisco J. Jiménez-Espejo, Alenjandro López-Avilés, R.Scott Anderson, Y. Y.: Paleohydrological dynamics in the
Western Mediterranean during the last glacial cycle, Glob. Planet. Change, 202, 2021.

Genty, D., Verheyden, S., Wainer, K., Speleothem records over the last interglacial. Investigating Past Interglacials, PAGES
news, 21, 1–2, 2013.

Gimeno, L., Nieto, R., Trigo, R. M., Vicente-Serrano, S. M., and López-Moreno, J. I.: Where does the Iberian Peninsula
moisture come from? An answer based on a Lagrangian approach, J Hydrometeorol, 11, 421–436,
https://doi.org/10.1175/2009JHM1182.1, 2010.

Gonzalez-Mora, B., Sierro, F. J., and Schönfeld, J.: Temperature and stable isotope variations in different water masses from
the Alboran Sea (Western Mediterranean) between 250 and 150 ka. Geochem. Geophys. Geosyst., 9, Q10016
https://doi.org/10.1029/2007GC001906, 2008.

Grant, K.M., Rohling, E.J., Bar-Matthews, M., Ayalon, A., Medina-Elizalde, M., Bronk Ramsey, C., Satow, C., Roberts, A.P.,
Rapid coupling between ice volume and polar temperature over the past 150 kyr. Nature, 491, 744-747. doi:
10.1038/nature11593, 2012.

Grant, K. M., Grimm, R., Mikolajewicz, U., Marino, G., Ziegler, M., & Rohling, E. J., The timing of Mediterranean sapropel
deposition relative to insolation, sea-level and African monsoon changes. Quaternary Science Reviews, 140, 125–141.
https://doi.org/10.1016/j.quascirev.2016.03.026, 2016.

Hellstrom J, McCulloch M, Stone J. A Detailed 31,000-Year Record of Climate and Vegetation Change, from the Isotope
Geochemistry of Two New Zealand Speleothems. *Quaternary Research*. 1998;50(2):167-178. doi:10.1006/qres.1998.

Hobart, B., Lisiecki, L. E., Rand, D., Lee, T., and Lawrence, C. E.: Late Pleistocene 100-kyr glacial cycles paced by precession
forcing of summer insolation, 16, https://doi.org/10.1038/s41561-023-01235-x, 2023.

Hodell, D.A., Channell, J.E.T., Curtis, J.H., Romero, O.E.,. Onset of '" Hudson Strait "' Heinrich events in the eastern North
Atlantic at the end of the middle Pleistocene transition 640ka. Paleoceanography, 23, 1–16. doi:10.1029/2008PA001591, 2008.

Hodell, D., Crowhurst, S., Skinner, L., Tzedakis, P. C., Margari, V., Channell, J. E. T., Kamenov, G., MacLachlan, S., and
Rothwell, G.: Response of Iberian Margin sediments to orbital and suborbital forcing over the past 420 ka, Paleoceanography,
28, 185–199, https://doi.org/10.1002/palo.20017, 2013.

Hodell, D., Lourens, L., Crowhurst, S., Konijnendijk, T., Tjallingii, R., Jiménez-espejo, F., Skinner, L., Shackleton, T., Project,
S., Abrantes, F., Acton, G. D., Zarikian, C. A. A., Bahr, A., Balestra, B., Barranco, E. L., Carrara, G., Ducassou, E., Flood, R.
D., Flores, J., Furota, S., Grimalt, J., Grunert, P., Hernández-molina, J., Kim, J. K., Krissek, L. A., Kuroda, J., Li, B., Lo, J.,
Margari, V., Martrat, B., Miller, M. D., Nanayama, F., Nishida, N., Richter, C., Rodrigues, T., Rodríguez-tovar, F. J., Cristina,
A., Roque, F., Goñi, M. F. S., Sánchez, F. J. S., Singh, A. D., Sloss, C. R., Stow, D. A. V, Takashimizu, Y., Tzanova, A.,
Voelker, A., Xuan, C., and Williams, T.: A reference time scale for Site U1385 (Shackleton Site) on the SW Iberian Margin.
Global and Planetary Change, 133, 49–64, https://doi.org/10.1016/j.gloplacha.2015.07.002, 2015.

Hodell, D. A., Crowhurst, S. J., Lourens, L., Margari, V., Nicolson, J., Rolfe, J. E., Skinner, L. C., Thomas, N. C., Tzedakis, P. C., Mleneck-Vautravers, M. J., and Wolff, E. W.: A 1.5-million-year record of orbital and millennial climate variability in the North Atlantic, Climate of the Past, 19, 607–636, https://doi.org/10.5194/cp-19-607-2023, 2023.

660 Imbrie, J., Hays, J.D., Martinson, D.G., McIntyre, A., Mix, A.C., Morley, J.J., Pisias, N.G., Prell, W.i Shackleton, N., The orbital theory of Pleistocene climate: support from a revised chronology of the marine d^{18}O record. Proceedings of the NATO Advanced Research Workshop on Milankovitch and Climate. D. Reidel Publishing Company, 269-305, 1984.

IPCC, 2023: Climate Change 2023: Synthesis Report. Contribution of Working Groups I, II and III to the Sixth Assessment Report of the Intergovernmental Panel on Climate Change [Core Writing Team, H. Lee and J. Romero (eds.). IPCC, Geneva, 665 Switzerland, 184 pp., doi: 10.59327/IPCC/AR6-9789291691647, 2023.

Jian, Z., Wang, Y., Dang, H., Mohtadi, M., Rosenthal, Y., Lea, D. W., Liu, Z., Jin, H., Ye, L., Kuhnt, W., and Wang, X.: Warm pool ocean heat content regulates ocean–continent moisture transport, Nature, 612, 92–99, https://doi.org/10.1038/s41586-022-05302-y, 2022.

Jiménez-Amat, P. and Zahn, R., Offset timing of climate oscillations during the last two glacial-interglacial transitions 670 connected with large-scale freshwater perturbation. Paleoceanography, 30, 768–788. doi:10.1002/2014PA002710, 2015.

Kaushal, N., Perez-Mejias, C., and Stoll, H. M.: Perspective on ice age Terminations from absolute chronologies provided by global speleothem records, Clim. Past Discuss. [preprint], https://doi.org/10.5194/cp-2024-37, 2024.

Krklec, K. and Domínguez-Villar, D., Quantification of the impact of moisture source regions on the oxygen isotope composition of precipitation over Eagle Cave, central Spain. Geoch. Cosm. Acta 134, 39-54. doi: 10.1016/j.gca.2014.03.011, 675 2014.

Kutzbach, J. E., Chen, G., Cheng, H., Edwards, R. L., and Liu, Z.: Potential role of winter rainfall in explaining increased moisture in the Mediterranean and Middle East during periods of maximum orbitally-forced insolation seasonality, 1079–1095, https://doi.org/10.1007/s00382-013-1692-1, 2014.

Lambeck, K., Rouby, H., Purcell, A., Sun, Y. & Sambridge, M. Sea level and global ice volumes from the Last Glacial 680 Maximum to the Holocene. Proceedings of the National Academy of Sciences 111, 15296-15303, 2014.

Laskar, J., Robutel, P., Joutel, F., Gastineau, M., Correia, A. C. M., and Levrard, B.: A long-term numerical solution for the insolation quantities of the Earth, Astron. Astrophys., 428, 261–285, https://doi.org/10.1051/0004-6361:20041335, 2004.

Lionello, P., The Climate of the Mediterranean Region: From the Past to the Future, 1st ed. Elsevier Inc. doi:10.1016/B978-0-12-416042-2.00009-4, 2012.

685 Lisiecki, L. E., and Raymo, M. E., A Pliocene-Pleistocene stack of 57 globally distributed benthic δ^{18}O records. Paleoceanography, 201, 1–17. https://doi.org/10.1029/2004PA001071, 2005.

Marino, G., Rohling, E.J., Rodríguez-Sanz, L., Grant, K.M., Heslop, D., Roberts, A.P., Stanford, J.D., Yu, J, Bipolar seesaw control on last interglacial sea level. Nature, 522, 197–201. doi:10.1038/nature14499, 2015.

Marra, F, Rohling, E.J., Florindo, F., Jicha, B., Nomade, S., Renne, P. R.: Independent 40 Ar / 39 Ar and 14 C age constraints

690   on the last five glacial terminations from the aggradational successions of the Tiber River , Rome (Italy), Earth Planet. Sci. Lett., 449, 105–117, https://doi.org/10.1016/j.epsl.2016.05.037, 2016.

Marra, F., Costantini, L., Buduo, G. M. Di, Florindo, F., Jicha, B. R., Palladino, D. M., and Sottili, G.: Combined glacio-eustatic forcing and volcano-tectonic uplift : Geomorphological and geochronological constraints on the Tiber River terraces in the eastern Vulsini Volcanic District (central Italy), Glob. Planet. Change, 182, 103009,

695   https://doi.org/10.1016/j.gloplacha.2019.103009, 2019.

Martinson, D. G., Pisias, N. G., Hays, J. D., Imbrie, J., Moore, T. C., and Shackleton, N. J., Age dating and the orbital theory of the ice ages: Development of a high-resolution 0 to 300,000-year chronostratigraphy. Quaternary research, 27(1), 1-29, 1987.

Martrat, B., Grimalt, J.O., Lopez-Martínez, C., Cacho, I., Sierro, F.J., Flores, J.A., Zahn, R., Canals, M., Curtis, J.H., Hodell,

700   D.A., Abrupt Temperature Changes in the Western Mediterranean over the Past 250,000 Years. Science, 306, 1762–1765. doi:10.1126/science.1101706, 2004.

Martrat, B., Grimalt, J.O., Shackleton, N.J., De Abreu, L., Hutterli, M.A., Stocker, T.F., Four climate cycles of recurring deep and surface water destabilizations on the Iberian margin. Science, 317, 502–507. doi:10.1126/science.1139994, 2007.

Milankovitch, M., Canon of Insolation and the Ice Age Problem. Royal Academy of Serbia 133, 633, 1941.

705   Millán, M.M., Estrela, J., Miró, J.: Rainfall Components : Variability and Spatial Distribution in a Mediterranean Area (Valencia Region), 2682–2705, 2005.

Moreno, A., Stoll, H., Jiménez-Sánchez, M., Cacho, I., Valero-Garcés, B., Ito, E., Edwards, R.L.,. A speleothem record of glacial 25-11.6 kyr BP. rapid climatic changes from northern Iberian Peninsula. Glob. Planet. Change, 71, 218–231. doi:10.1016/j.gloplacha.2009.10.002, 2010.

710   Moreno, A., Iglesias, M., Azorin-molina, C., Pérez-mejías, C., Bartolomé, M., Sancho, C., Stoll, H., Cacho, I., Frigola, J., Osácar, C., and Muñoz, A.: Measurement report : Spatial variability of northern Iberian rainfall stable isotope values – investigating atmospheric controls on daily and monthly timescales, 10159–10177, 2021.

Moseley, G. E., Edwards, R. L., Wendt, K. A., Cheng, H., Dublyansky, Y., Lu, Y., Boch, R..: Reconciliation of the Devils Hole climate record with orbital forcing, Science (1979), 351, 165–168, 2016.

715   Nichols, M. D., Xuan, C., Crowhurst, S., Richter, C., Acton, G. D., and Wilson, P. A.: Climate - Induced Variability in Mediterranean Out fl ow to the North Atlantic Ocean During the Late Pleistocene Paleoceanography and Paleoclimatology, 1–17, https://doi.org/10.1029/2020PA003947, 2020.

Nieto, R., Gimeno, L., Drumond, A., Hernandez, E., A Lagrangian identification of the main moisture sources and sinks affecting the Mediterranean area. WSEAS Trans. Env. and Dev. 6, 365-374, 2010.

720   Ochoa, D., Sierro, F. J., Hilgen, F. J., Cortina, A., Lofi, J., Kouwenhoven, T., and Flores, J. A.: Origin and implications of orbital-induced sedimentary cyclicity in Pliocene well-logs of the Western Mediterranean, Mar. Geol., 403, 150–164, https://doi.org/10.1016/j.margeo.2018.05.009, 2018.

Paillard, D., Labeyric, L. & Yiou, P., Machintosh program performs time-series analysis. Eos Transactions, AGU 77,376, 1996.

725 PAGES, P.I.W.G. of P., Interglacials of the last 800,000years. Rev. Geophys. 54, 162–219. doi:10.1002/2015RG000482, 2016.

Pérez-Mejías, C., Moreno, A., Sancho, C., Bartolomé, M., Stoll, H., Cacho, I., Cheng, H., & Edwards, R. L., Abrupt climate changes during Termination III in Southern Europe. Proceedings of the National Academy of Sciences of the United States of America, 11438, 10047–10052. https://doi.org/10.1073/pnas.1619615114, 2017.

Rahmstorf, S.: Ocean circulation and climate during the past 120,000 years, Nature, 419, 207–214,
730 https://doi.org/10.1038/nature01090, 2002

Rohling, E.J., Foster, G.L., Grant, K.M., Marino, G., Roberts, A.P., Tamisiea, M.E., Williams, F.,. Sea-level and deep-sea-temperature variability over the past 5.3 million years. Nature 508, 477-482. doi: 10.1038/nature13230, 2014.

Rohling, E. J., Marino, G., and Grant, K. M., Mediterranean climate and oceanography, and the periodic development of anoxic events sapropels. Earth-Science Reviews, 143, 62–97. https://doi.org/10.1016/j.earscirev.2015.01.008, 2015.

735 Sánchez-Goñi, M.F., Eynaud, F., Turon, J.L., Shackleton, N.J., High resolution palynological record off the Iberian margin: Direct land-sea correlation for the Last Interglacial complex. Earth Planet. Sci. Lett. 171, 123–137. doi:10.1016/S0012-821X99.00141-7, 1999.

Sánchez-Goñi, M. F., Landais, A., Fletcher, W.J., Naughton, F., Desprat, S., Duprat, J.: Contrasting impacts of Dansgaard – Oeschger events over a western European latitudinal transect modulated by orbital parameters, Quat. Sci. Rev., 27, 1136–
740 1151, https://doi.org/10.1016/j.quascirev.2008.03.003, 2008.

Schicker, I., Radanovics, S., and Seibert, P.: Origin and transport of mediterranean moisture and air, Atmos. Chem. Phys., 10, 5089–5105, https://doi.org/10.5194/acp-10-5089-2010, 2010.

Scholz, D., Hoffmann, D.L., StalAge: An algorithm designed for construction of speleothem age models. Quat. Geoch. 6, 369–382. doi:10.1016/j.quageo.2011.02.002, 2011.

745 Shackleton, N. J., The last interglacial in the marine and terrestrial records. Proceedings of the Royal Society of London. Series B. Biological Sciences, 1741034, 135-154, 1969.

Shackleton, N. J., Sánchez-Goñi, M. F., Pailler, D., and Lancelot, Y.: Marine isotope substage 5e and the Eemian interglacial, Glob. Planet. Change, 36, 151–155, https://doi.org/10.1016/S0921-8181(02)00181-9, 2003.

Shen, C., Edwards, R.L., Cheng, H., Dorale, J.A., Thomas, R.B., Moran, S.B., Weinstein, S.E., Edmonds, H.N., Uranium and
750 thorium isotopic and concentration measurements by magnetic sector inductively coupled plasma mass spectrometry. Chem. Geo. 185, 165–178, 2002.

Sierro, F.J., Hodell, D.A., Curtis, J.H., Flores, J.A., Reguera, I., Colmenero-Hidalgo, E., Barcena, M.A., Grimalt, J.O., Cacho, I., Frigola, J., Canals, M., Impact of iceberg melting on Mediterranean thermohaline circulation during Heinrich events. Paleoceanography 20, 1–13. doi:10.1029/2004PA001051, 2005.

755 Sierro, F. J., Hodell, D. A., Andersen, N., and Azibeiro, L. A.: Mediterranean Over fl ow Over the Last 250 kyr : Freshwater Forcing From the Tropics to the Ice Sheets Paleoceanography and Paleoclimatology, 1–31, https://doi.org/10.1029/2020PA003931, 2020.

Skinner, L. & Shackleton, N. Deconstructing Terminations I and II: revisiting the glacioeustatic paradigm based on deep-water temperature estimates. Quaternary Science Reviews 25, 3312- 3321, 2006.

760 Spötl, C., Scholz, D., and Mangini, A., A terrestrial U/Th-dated stable isotope record of the Penultimate Interglacial. Earth and Planetary Science Letters, 2763–4., 283–292. https://doi.org/10.1016/j.epsl.2008.09.029, 2008.

Stoll, H. M., Müller, W., and Prieto, M.: I-STAL, a model for interpretation of Mg/Ca, Sr/Ca and Ba/Ca variations in speleothems and its forward and inverse application on seasonal to millennial scales, Geochemistry, Geophys. Geosystems, 13, https://doi.org/10.1029/2012GC004183, 2012.

765 Stoll, H., Mendez-Vicente, A., Gonzalez-Lemos, S., Moreno, A., Cacho, I., Cheng, H., Edwards, R.L., Interpretation of orbital scale variability in mid-latitude speleothem d 18 O : Significance of growth rate controlled kinetic fractionation effects. Quat. Sci. Rev. 127, 215–228. doi:10.1016/j.quascirev.2015.08.025, 2015.

Stoll, H. M., Cacho, I., Gasson, E., Sliwinski, J., Kost, O., Iglesias, M., Torner, J., Perez-Mejias, C., Haghipour, N., Cheng, H., Edwards, R. L., and Moreno, A.: Rapid northern hemisphere ice sheet melting during the penultimate deglaciation, Nat
770 Commun, 13, 3819, https://doi.org/10.1038/s41467-022-31619-3, 2022.

Toucanne, S., Angue Minto'o, C. M., Fontanier, C., Bassetti, M. A., Jorry, S. J., and Jouet, G., Tracking rainfall in the northern Mediterranean borderlands during sapropel deposition. Quaternary Science Reviews, 129, 178–195. https://doi.org/10.1016/j.quascirev.2015.10.016, 2015.

Torner, J., Cacho, I., Moreno, A., Sierro, F. J., Martrat, B., Rodriguez-Lazaro, J., Frigola, J., Arnau, P., Belmonte, Á.,
775 Hellstrom, J., Cheng, H., Edwards, R. L., and Stoll, H.: Ocean-atmosphere interconnections from the last interglacial to the early glacial: An integration of marine and cave records in the Iberian region, Quat. Sci. Rev., 226, https://doi.org/10.1016/j.quascirev.2019.106037, 2019.

Tzedakis, C., 2003. Timing and duration of Last Interglacial conditions in Europe: A chronicle of a changing chronology. Quat. Sci. Rev. 22, 763–768. doi:10.1016/S0277-379103.00004-0.

780 Tzedakis, P. C., Hooghiemstra, H., and Pälike, H., The last 1.35 million years at Tenaghi Philippon: revised chronostratigraphy and long-term vegetation trends. Quaternary Science Reviews, 2523–24, 3416–3430. https://doi.org/10.1016/j.quascirev.2006.09.002, 2006.

Tzedakis, P.C., Raynaud, D., McManus, J.F., Berger, A., Brovkin, V., Kiefer, T., 2009. Interglacial diversity. Nat. Geosci. 2, 751, 2009.

785 Tzedakis, P.C., Wolff, E.W., Skinner, L.C., Brovkin, V., Hodell, D.A., McManus, J.F., Raynaud, D.,. Can we predict the duration of an interglacial? Clim. Past 8, 1473–1485. doi:10.5194/cp-8-1473-2012, 2012.

Tzedakis, P. C., Crucifix, M., Mitsui, T., and Wolff, E. W.: A simple rule to determine which insolation cycles lead to interglacials, Nat. Publ. Gr., 542, 427–432, https://doi.org/10.1038/nature21364, 2017.

Tzedakis, P.C., Drysdale, R.N., Margari, V., Skinner, L.C., Menviel, L., Rhodes, R.H., Taschetto, A.S., Hodell, D.A., Crowhurst, S.J., Hellstrom, J.C., Fallick, A.E., Grimalt, J.O., McManus, J.F., Martrat, B., Mokeddem, Z., Parrenin, F., Regattieri, E., Roe, K., Zanchetta, G., Enhanced climate instability in the North Atlantic and southern Europe during the Last Interglacial. Nat. Commun. 9, 4235. doi:10.1038/s41467-018-06683-3, 2018.

Waelbroeck, C., Kiefer, T., Dokken, T., Chen, M. T., Spero, H. J., Jung, S., Weinelt, M., Kucera, M., and Paul, A.: Constraints on surface seawater oxygen isotope change between the Last Glacial Maximum and the Late Holocene, Quat Sci Rev, 105, 102–111, https://doi.org/10.1016/j.quascirev.2014.09.020, 2014.

Wagner, B., Vogel, H., Francke, A., Friedrich, T., Donders, T., Lacey, J. H., Leng, M. J., Regattieri, E., Sadori, L., Wilke, T., Zanchetta, G., and Albrecht, C.: monsoons during the past 1 . 36 million years, Nature, https://doi.org/10.1038/s41586-019-1529-0, 2019.

Wang, C., A unified oscillator model for the El Niño-Southern Oscillation. Journal of Climate, 14, 98-115, 2001.

Wendt, K. A., Li, X., Edwards, R. L., Cheng, H., and Spötl, C.: Precise timing of MIS 7 sub-stages from the Austrian Alps, 1–19, 2020.

Yuan D., Cheng H., Edwards R. L., Dykoski C. A., Kelly M. J., Zhang M., Qing J., Lin Y., Wang Y., Wu J., Dorale J. A., An Z. and Cai Y., Timing, Duration, and Transitions of the Last Interglacial Asian Monsoon. Science 304, 575–578, 2004.